CERN-ACC-2016-0334

2016-12-12

edmundo.lopez.sola@cern.ch

Preliminary AD-Horn Thermomechanical and Electrodynamic Simulations

Edmundo Lopez Sola / EN-STI, David Horvath / EN-STI, Marco Calviani / EN-STI

Keywords: AD horn, inner conductor, thermomechanical, ANSYS®, Maxwell®, metrology

Summary

As part of the Antiproton Decelerator (AD) target area consolidation activities planned for LS2, it has been necessary to perform a comprehensive study of the thermo-structural behaviour of the AD magnetic horn during operation, in order to detail specific requirements for the upgrade projects and testing procedures. The present work illustrates the preliminary results of the finite element analysis carried out to evaluate the thermal and structural behaviour of the device, as well as the methodology used to model and solve the thermomechanical and electrodynamic simulations performed in the AD magnetic horn.

1. Introduction

The present note describes the thermal, mechanical and electromagnetic simulations carried out in the currently installed AD magnetic horn. During the operation in the AD Target area, the AD horn is under high thermal and structural stresses from different origins, which can be especially critical in the horn inner conductor. Through finite element simulations with ANSYS® we have studied the thermal and structural response of the magnetic horn during operation, under high-intensity current pulse and particle beam interaction.

This note starts with a description of the AD Horn operation in the AD Target area, and then details the AD Horn inner conductor modelling in ANSYS®. Then, the electric analysis and the beam energy deposition application to the inner conductor are explained, in order to understand the full thermal analysis presented in chapter 6. The structural behaviour of the inner conductor is analysed in the next chapter, and finally the use of the electromagnetic simulation software Maxwell® is presented for a better understanding of this analysis. This note is a follow-up and an update of the work done in Ref. [1], where the presently operating horn is described.

2. AD Horn description and operation

The AD magnetic horn is located in the AD target area, where the antiprotons are produced in order to be injected into the antiproton decelerator (AD) ring. Its main purpose is to focus the diverging antiproton beam generated in the production target.

The 26 GeV/c proton beam extracted from the Proton Synchrotron (PS) impacts the AD production target, and the nuclear interactions between the proton beam and the spallation material of the target (iridium at the present time) are responsible for the production of secondary particles (among which anti-protons). The secondary particles emerge from the target with a given momentum and angular distribution, and the charged particles entering the

magnetic volume generated in the horn can be deviated into a parallel beam. This volume is enclosed between two coaxial conductors, the outer conductor being responsible for carrying the current to and from the inner conductor. The biconical "horn" shape of the inner conductor produces a toroidal magnetic volume between the two conductors where the entering charged particles are bent by the magnetic field and focused (in the case of antiprotons) in the forward direction (Fig.1).

Figure 1 Horn assembly and schematic of beam focusing, Ref. [1]

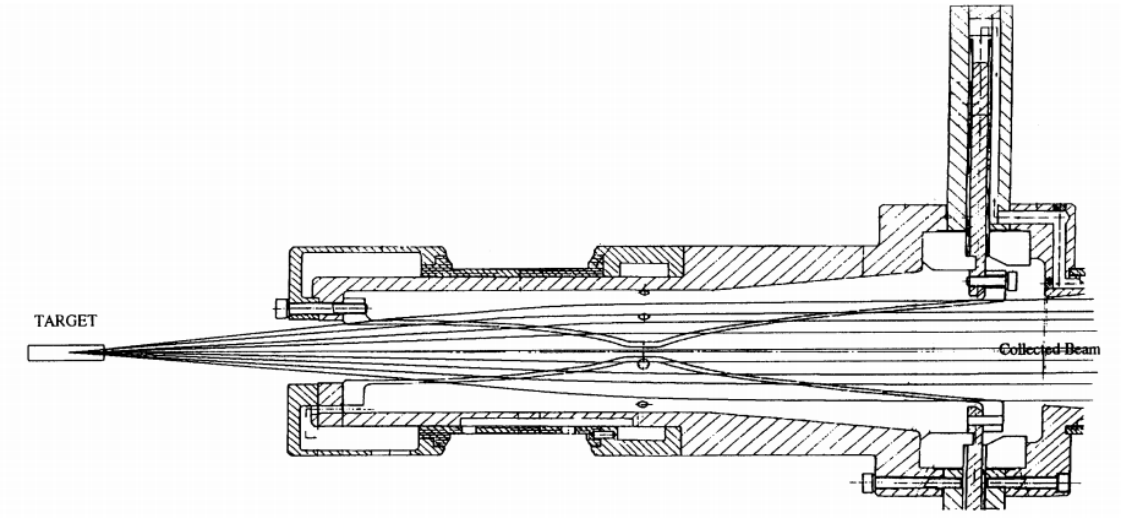

The horn is pulsed with a current of maximum intensity 400 kA, synchronized with the PS beam arriving to the target. A high-current pulser using a capacitor discharge circuit is responsible for the power supply of the stripline, which carries the current to the inner conductor [1][2]. In the following image the AD horn power supply circuit is described, showing the 18 ignitron cubicles that provide an intensity of 400 kA to the horn through the stripline (Fig.2).

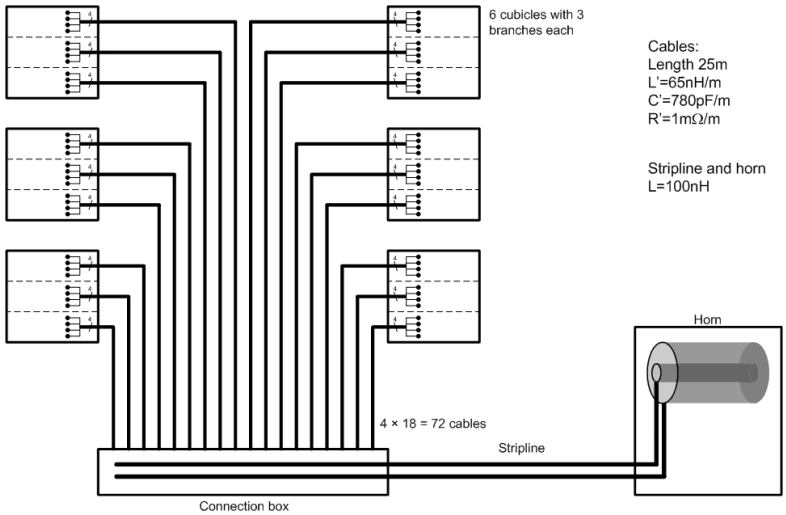

Figure 2 AD horn power supply circuit layout

The magnetic horn inner conductor material is a high strength alluminium alloy AA7075-T6 (also known as Perunal-215), chosen for its high tensile strength under dynamic stresses, since the horn should resist high mechanical loads and work in an intense radiation field. The material properties of this alluminium alloy are obtained from the software MPDB (Material Properties Database) [5], that provides the properties that have to be considered for the electric, thermal and structural analysis, and their evolution in function of the temperature.

The thickness of the inner conductor has been optimized in order to be as small as possible to decrease the antiproton reabsorption, but without compromising the mechanical

integrity of the horn during the pulsing process; with a resulting thickness of 3.5 mm in the neck of the horn and 1.4 mm in the wide end downstream.

Due to the high temperatures reached in the horn (as shown in the following chapters), an air-cooling system is included in the design, with an air-flow of 15 m^3/h passing between the inner conductor and the outer housing.

The high intensity current pulse generates thermal loads in the horn, as well as strong electromagnetic body forces due to the toroidal magnetic field; and the interactions between the secondary particles and the inner and outer conductor are also origin of thermal stresses. In the following sections, thermomechanical and electrodynamic analysis will be carried out, in order to identify and locate the thermal and mechanical stresses in the AD horn.

3. AD-Horn inner conductor modelling in ANSYS®

The horn shape is modelled with help of CAD-software according to the data included in the horn drawings, listed in EDMS 1180248 (https://edms.cern.ch/document/1180248/1) [2]. This geometry is included in ANSYS® Workbench (Fig.3) in order to perform the first set of electrodynamic and thermomechanical simulations, without considering the outer conductor for reasons of simplicity.

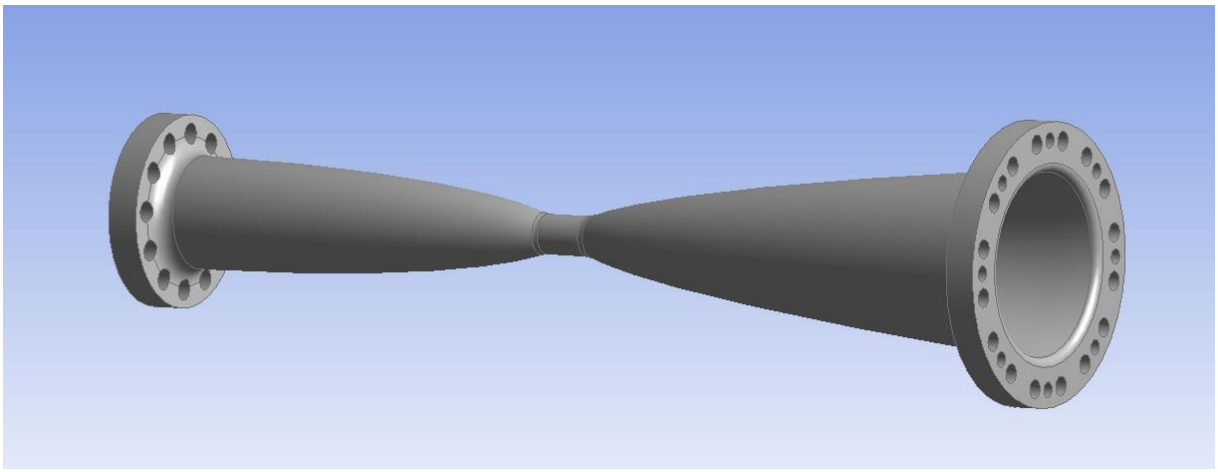

Figure 3 Inner conductor model imported in ANSYS®

The different attempts to obtain an accurate mesh in the horn, especially in the central narrow part, have shown that dividing the inner conductor geometry in three parts allows a better meshing. The supporting parts where the screws and cooling system holes are placed, require a higher mesh complexity, and have to be separated from the central part which has a more regular shape.

With this operation, we can easily obtain hexagonal elements in the parabolic, elliptical and cylindrical parts, whose size can be modified to generate a finer mesh. In the other hand, in the support parts, where the mesh accuracy is not that relevant, the obtained elements have a tetrahedral shape (Fig.4).

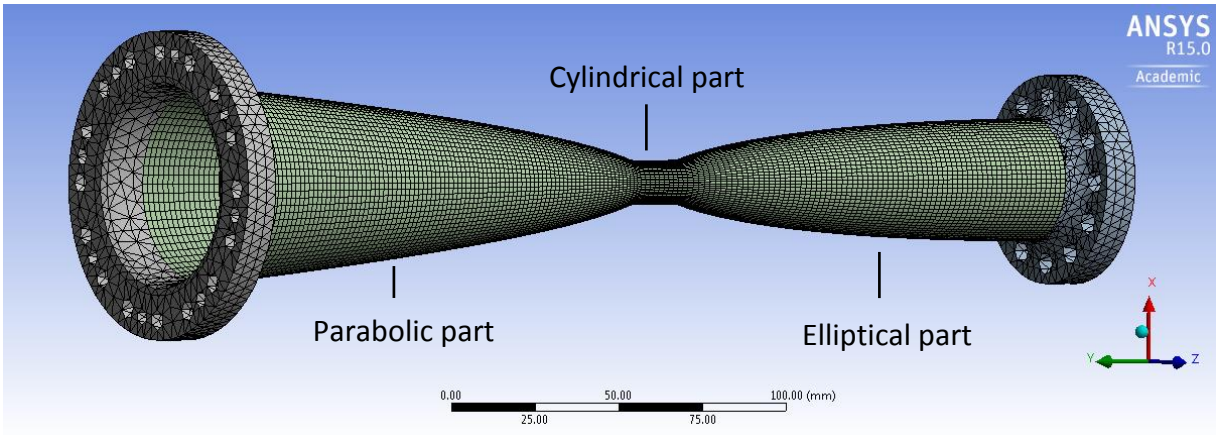

Figure 4 Inner conductor meshing overview

The possibility of meshing the central part of the horn with small elements by specifying the element size in the meshing control options should be considered specially to obtain more than one single element in the thickness of the horn. The problematic issue in this case is the fact that having more than one element in the thickness increases substantially the total number of elements of the mesh (Fig.5). Thus, another solution have been considered to reduce the number of elements and therefore the computational time of the simulations, i.e. by using an axisymmetric approach of the model.

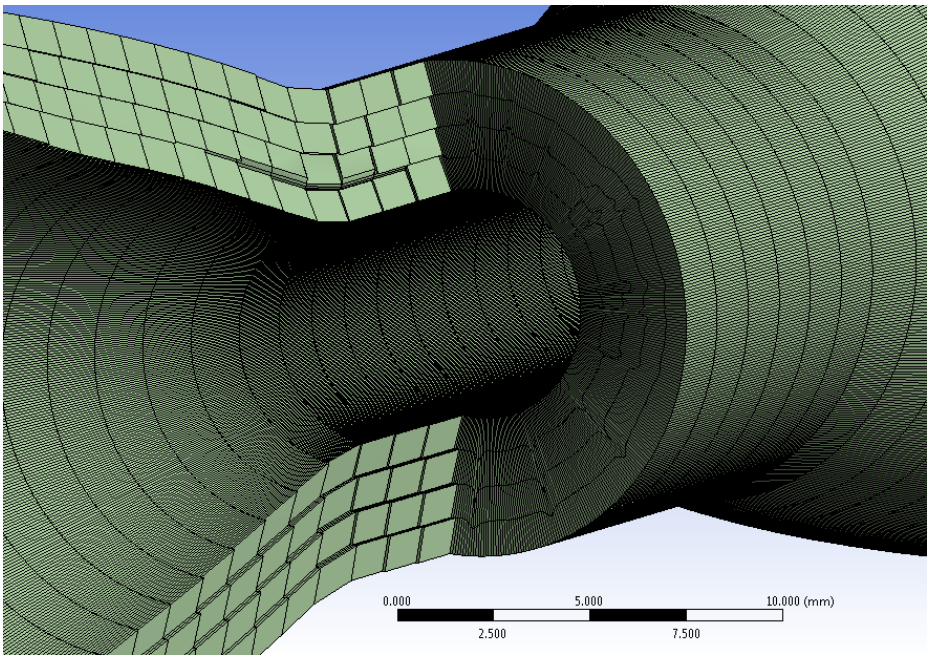

Figure 5 Meshing with four elements in the thickness of the horn

Reducing the horn model to an axisymmetric shape allows decreasing the computational time while having many elements in the thickness of the horn (Fig.6). The axisymmetric model has been therefore used generally for all the simulations, although the whole model shape have been considered regularly for crosschecking the results. Particularly for the analysis of the dynamic behaviour of the horn, the whole shape of the horn must be taken into account, given that it may be possible to have non-axisymmetric modes of deformation in the inner conductor.

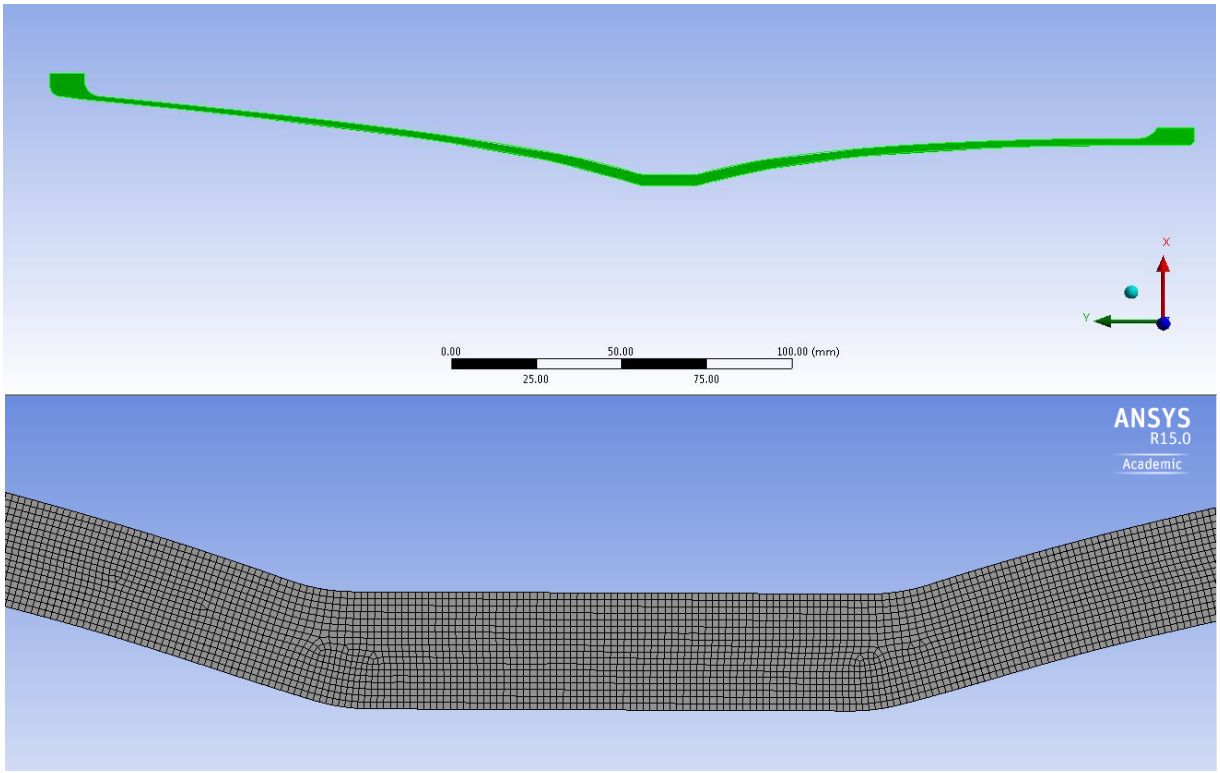

Figure 6 Axisymmetric reduction of the horn shape
Increased number of elements in the thickness of the horn

4. Electric Analysis of the AD magnetic horn

The Joule heat generated by the high current pulsed from the strip-line to the horn can be obtained by performing an electric analysis in ANSYS® Workbench. Applying the necessary current and voltage boundary conditions allow us to obtain the generated Joule heating in the inner conductor.

4.1 Electric resistivity

The property to be defined in order to carry out the electric analysis is the resistivity of the aluminium alloy AA7075-T6 in Ω·m. In the analysis, the Joule heating will be obtained for each element by taking into account the current applied and the resistance of the element (calculated according to the resistivity).

Since the resistivity evolution with temperature provided by the MPDB software [5] only includes a range under the ambient temperature, the resistivity considered is 52.2 nΩ·m, which is the value for the AA7075-T6 at room temperature [3]. This property varies with the temperature though, therefore a further study on the variation of the resistivity versus temperature must be carried out in the future.

4.2 Boundary conditions

The current pulse coming from the strip-line is applied on the inner face of the support part in the wide end of the horn inner conductor, according to the horn drawings. It has been necessary to define as well a ground voltage boundary condition for this analysis to be carried out, which will be placed in the opposite end of the horn, as shown in the drawings (Fig.7).

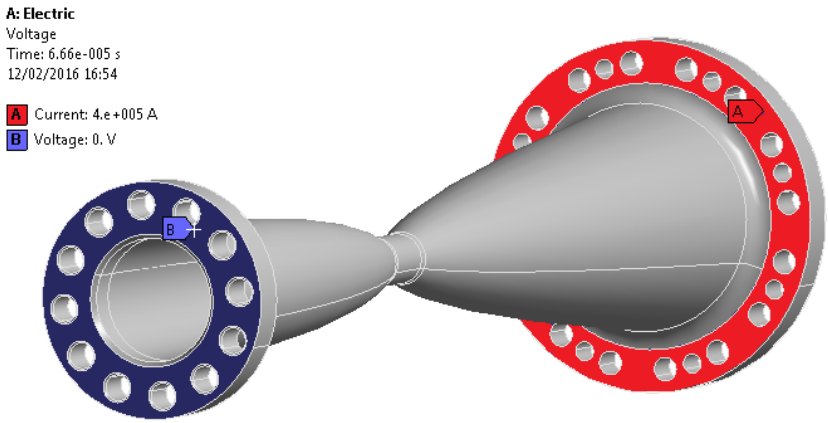

Figure 7 Current and voltage applied to the magnetic horn

It is possible to obtain real data of the current pulse shape by summing up the current values of each one of the 18 ignitrons integrated in the capacitor discharge circuit, recorded during the AD-Target area operation at a specific selected time. Taking a time span of 200 μs, we will consider a sample of 10000 values of real current stored, which are included as tabular data to represent the current input in the electrical analysis (see Fig.8 for a real current pulse). This is an approximation of the current shape that is repeated pulse by pulse in the magnetic horn.

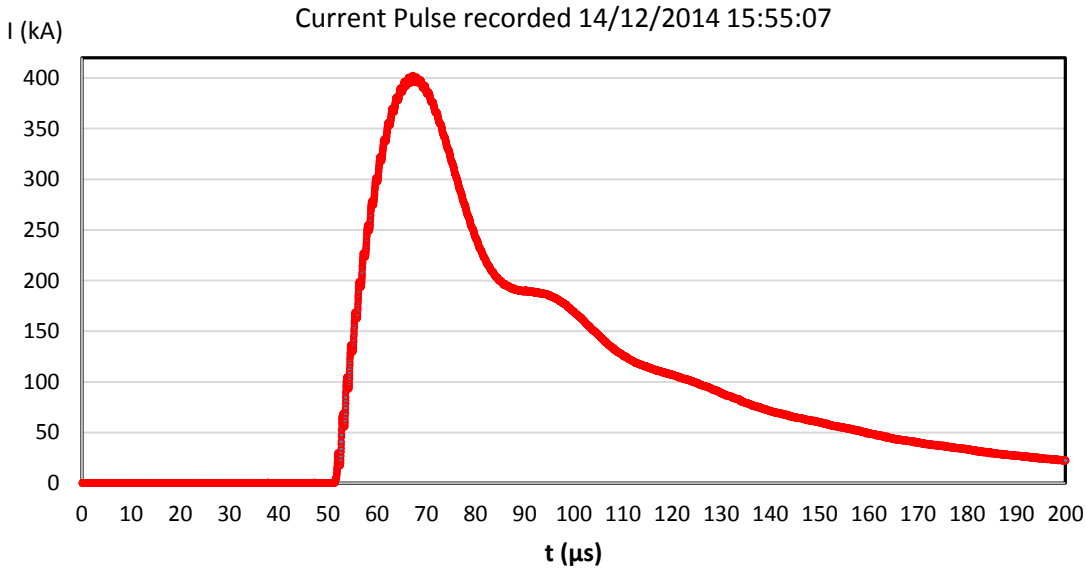

Figure 8 Real current pulse data obtained from the circuit's ignitrons

4.3 Results: Joule heating distribution

After having performed the electrical analysis, we can obtain the variation with the time of the Joule heating distribution along the horn, and by coupling these results with a thermal analysis we will be able to calculate the temperature variation provoked by the current pulse. The Joule heating is given in W/mm^3, and its evolution during the current pulse is very similar to the shape of the current, with the time of maximum heating corresponding with the current peak (Fig.9).

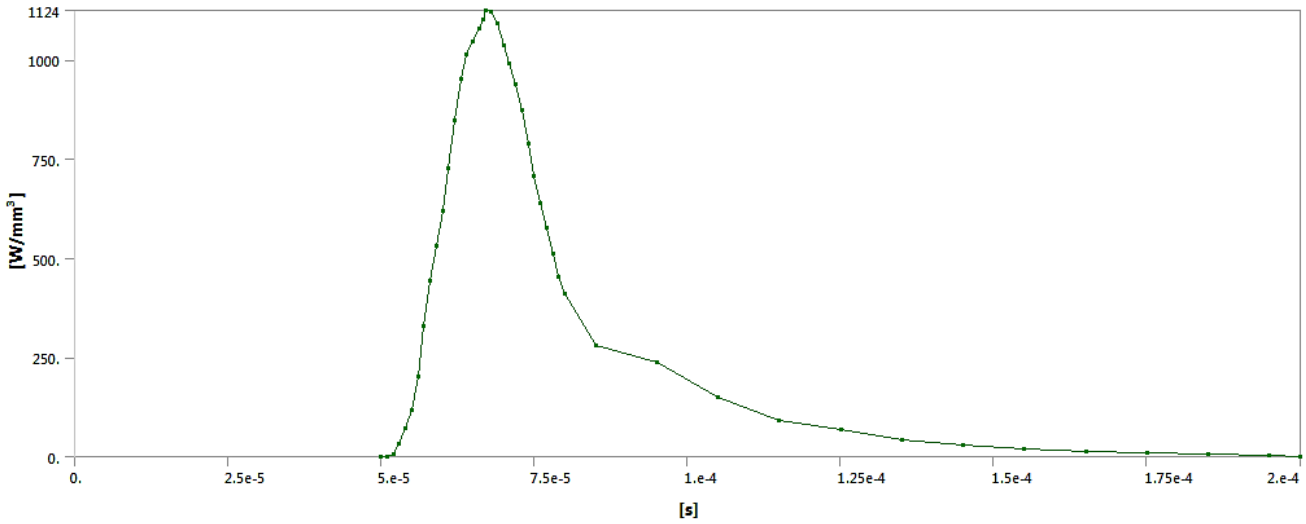

Figure 9 ANSYS results for the maximum Joule heating evolution during 200 µs

The maximum Joule heating, obtained at the current peak, is located in the edges of the neck of the horn, in the outer surface of the inner conductor (Fig.10). It can be seen that considering less elements in the thickness of the horn, it wouldn't be possible to appreciate this detail of energy distribution.

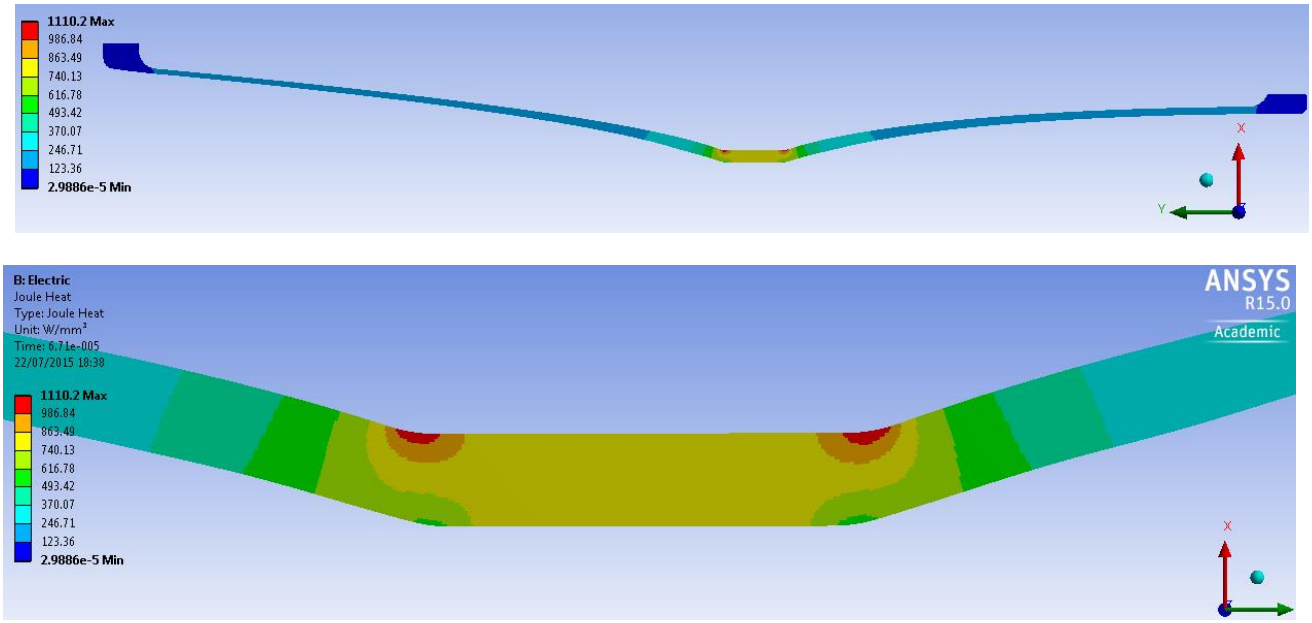

Figure 10 Joule heating distribution in the horn at the current peak in W/mm^3

4.4 Thermal coupling

The Joule heating distribution in the inner conductor can be transferred to a thermal transient analysis, where the values at the different time-steps are included as internal heat generation in W/mm^3. Performing the thermal transient analysis would provide, as a result, the temperature evolution in the horn only considering the heat generated by the current pulse.

At the end of the current pulse, after 200 µs and assuming 22 °C as ambient temperature, the temperature in the inner conductor has raised to a maximum of around 33.5°C in the neck of the horn, exactly where the maximum Joule heat was obtained (Fig.11 and 12).

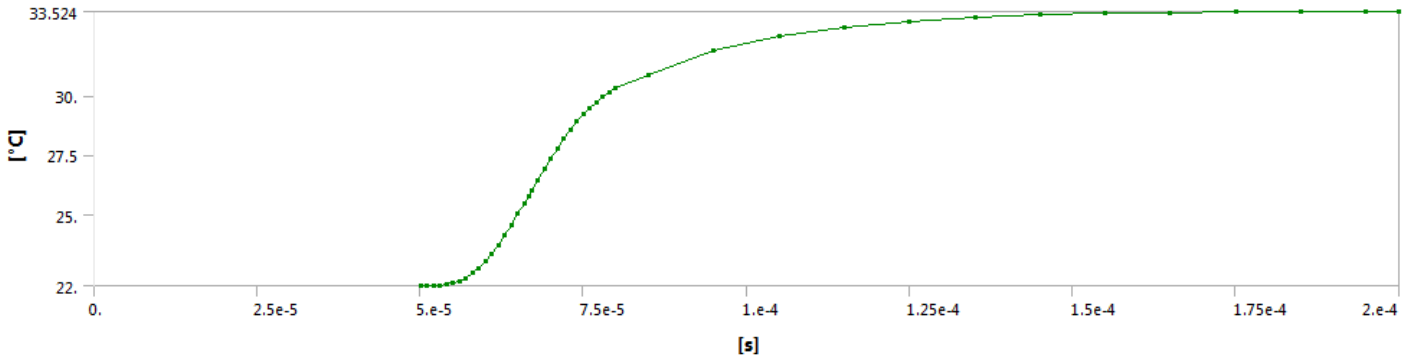

Figure 11 Maximum temperature evolution, only Joule heating considered

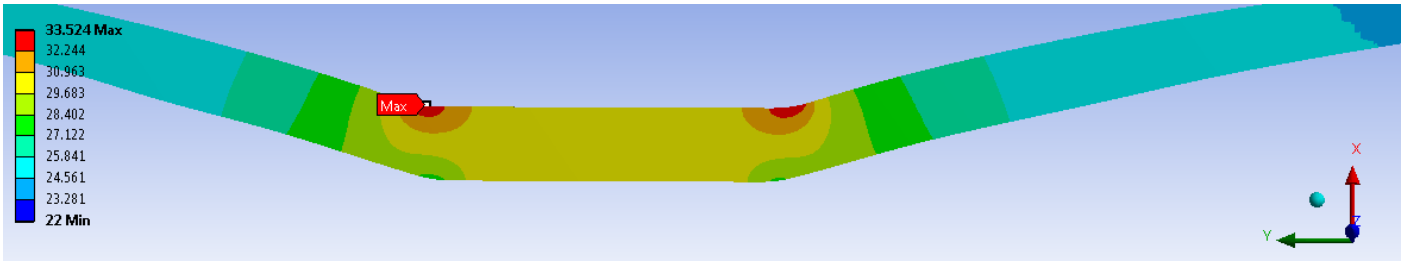

Figure 12 Temperature distribution in °C in the inner conductor after 200 µs, only Joule effect

4.5 Total heat generated

According to the measurements carried out in the past, the electrical resistance of the AD horn inner conductor is around 110 µΩ [1]. The total power generated in the horn by the current pulse at the peak (400 kA) can be calculated as follows: $P = I^2R = (400 \cdot 10^3 A)^2 \cdot 110 \cdot 10^{-6}\ \Omega = 17.6\ MW$.

This value can also be obtained in an electrical analysis performed in ANSYS® Workbench with help of ANSYS Parametric Design Language (APDL) commands. The code shown in Annex A.1 allows to obtain the volume and the Joule heating in W/mm^3 for each element of the horn model, and multiply them to obtain the power in W of each element.

Then, all the values calculated are summed up to obtain the total heat generated in the horn (only by the current pulse) according to the electrical analysis performed, as shown in **Table 1.**

The obtained total heat of 14.2 MW differs from the theoretically calculated power (17.6 MW), despite being of the same order of magnitude. These results depend strongly on the resistivity value used, and the inner conductor resistance as calculated in ANSYS® is around 90 µΩ, quite different to the obtained in the past (110 µΩ).

Table 1 - Extract from the tables created with the APDL commands and total heat

Heat generation (W/mm^3)	**Volume ($\cdot 10^3\ mm^3$)**	**Total Heat (W)**	**Total Heat Generation (MW)**
0.17	4.0	684	**14.2**
0.12	4.4	552	
0.22	2.5	555	
0.20	1.9	374	
0.15	4.3	638	
0.28	1.1	323	
…	…	…	

In order to check the real resistance of the inner conductor, new measurements have been carried out in collaboration with TE/ABT, and the obtained value is 66 μΩ. This electrical resistance is significantly lower than the value measured for the old horn consolidation [1]. According to this resistance, the total heat generated in the horn at the current peak is 10.6 MW, hence the thermal calculations performed are conservative.

5. Beam energy deposition in the AD Horn

The energy deposition expected in the inner conductor by the interaction of the particles generated after the AD Target has been calculated by means of the FLUKA Monte Carlo code [6, 7]. The energy distribution obtained (Fig.13) can be simplified by considering the axisymmetric shape of the horn.

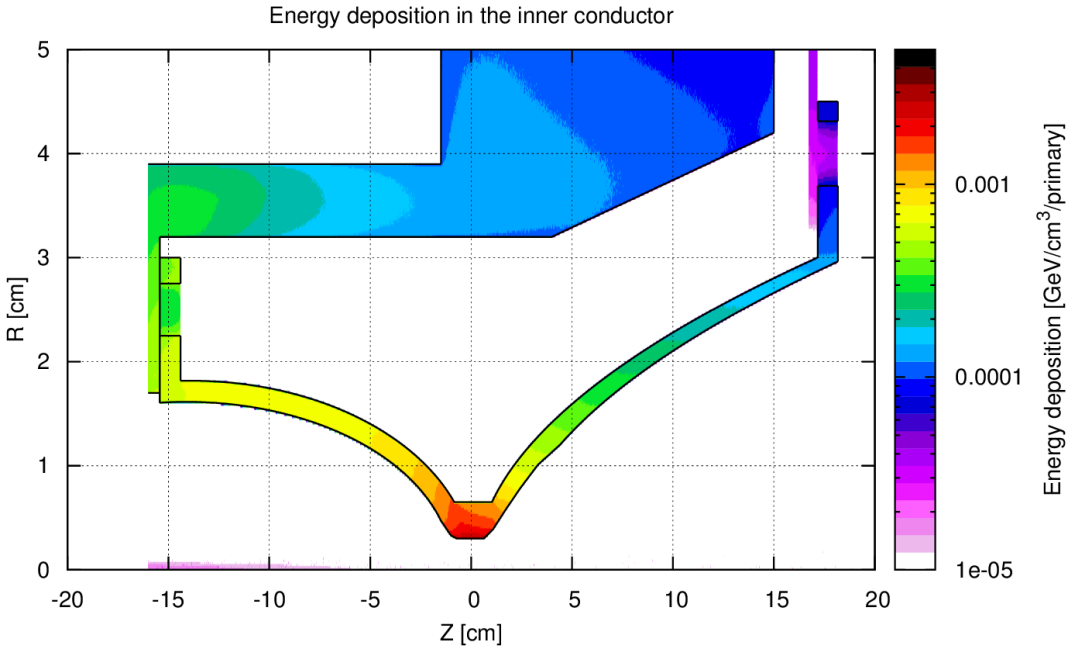

Figure 13 Energy deposition per primary proton in target in the inner conductor - FLUKA simulations results

The data is given in function of the Z-coordinate, and a conservative approach will be made by considering for each interval [z_1, z_2] with length 0.2 mm the maximum energy deposition in this interval. The energy distribution applied to our model will be then as shown in Fig. 14, taking values each 0.2 mm steps.

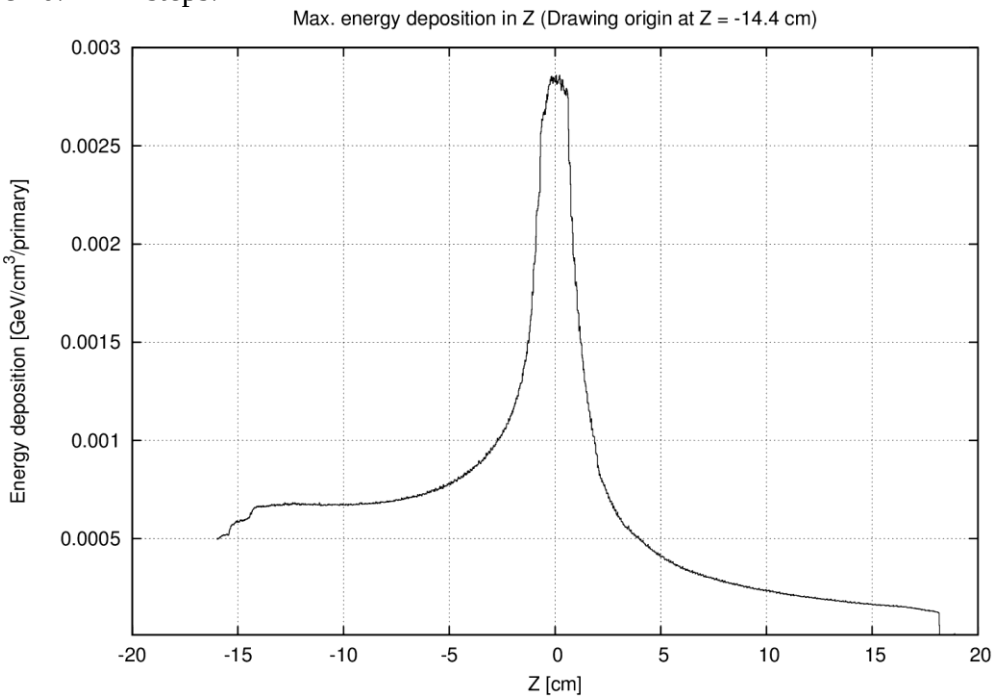

Figure 14 FLUKA calculated maximum energy deposition (function of Z-coordinate)

The results obtained with FLUKA are included as External Data in ANSYS® Workbench, and imported into a Transient Thermal Analysis as Internal Heat Generation (in W/mm^3). In order to convert the data provided by the FLUKA results which are expressed in GeV/cm^3/proton, we need to consider that each pulse lasts about 500 ns (a good approximation of the 4 bunches sent to the AD-target by the Proton Synchrotron machine) and contains around $1.5 \cdot 10^{13}$ protons.

Then, we can import the converted results to the meshed model in ANSYS® obtaining the energy deposition distribution in W/mm^3 (Fig.15).

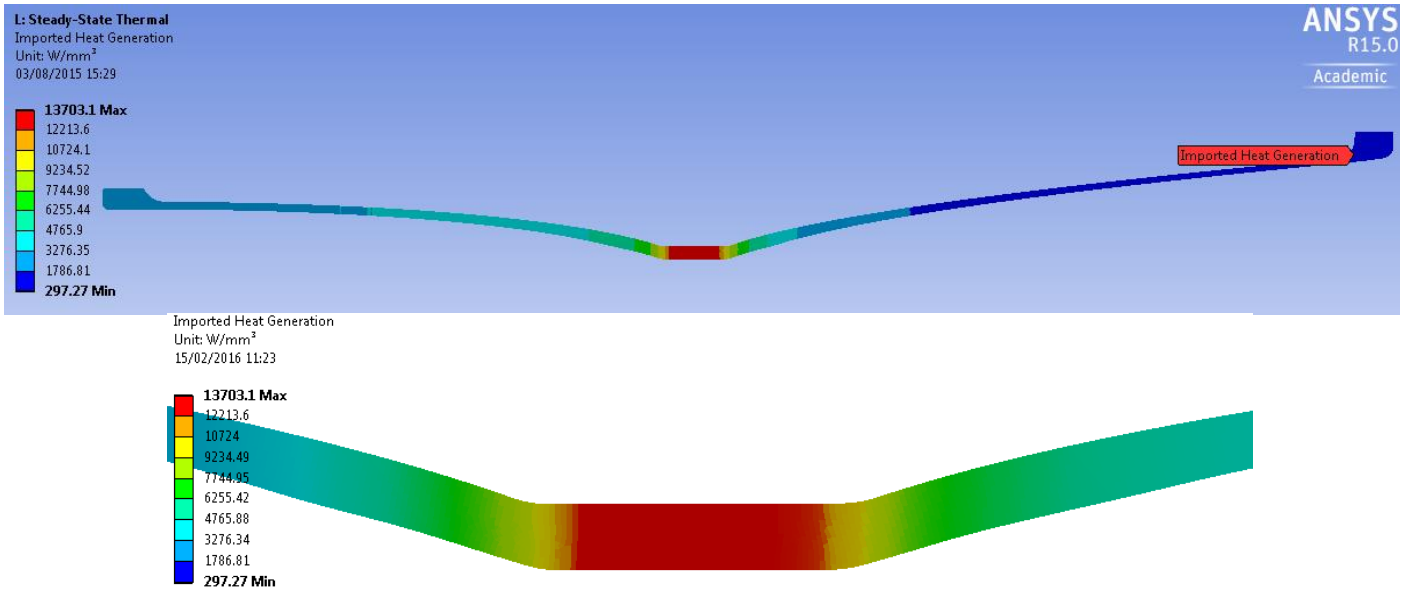

Figure 15 Imported energy deposition in ANSYS®

As a first approach, it is possible to simulate the temperature increase due only to the beam energy deposition. For that purpose, the energy is imported as a stepped load lasting 500 ns, and the temperature increases therefore linearly until a maximum temperature of about 25 °C (i.e. a differential temperature of 3 °C per pulse, Fig.16).

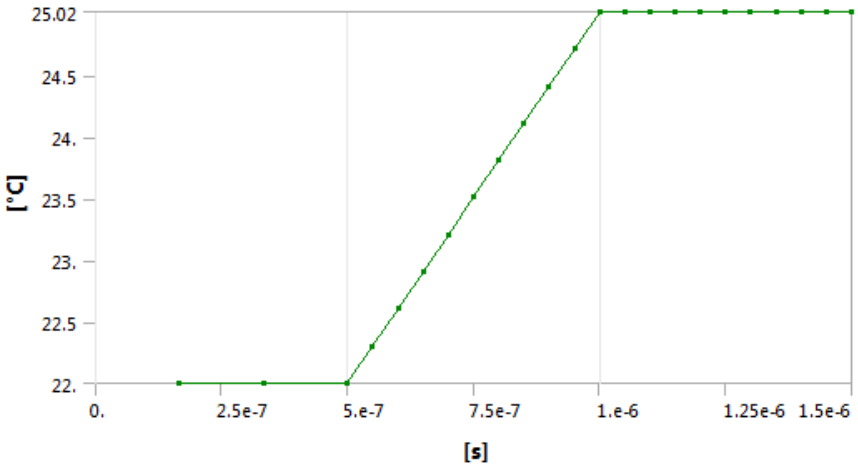

Figure 16 Maximum temperature evolution considering only the energy deposition induced by the proton beam and the secondaries.

6. AD horn full thermal analysis

6.1 Total thermal loads

Once the Joule heating produced by the current pulse and the energy deposited by the beam are obtained, it is necessary to include both thermal loads in a transient thermal analysis. In order to perform this analysis, we will consider that the beam pulse takes place at the same time as the current peak is generated (Fig. 17), as the strongest magnetic field will be created when the current reaches its 400 kA peak.

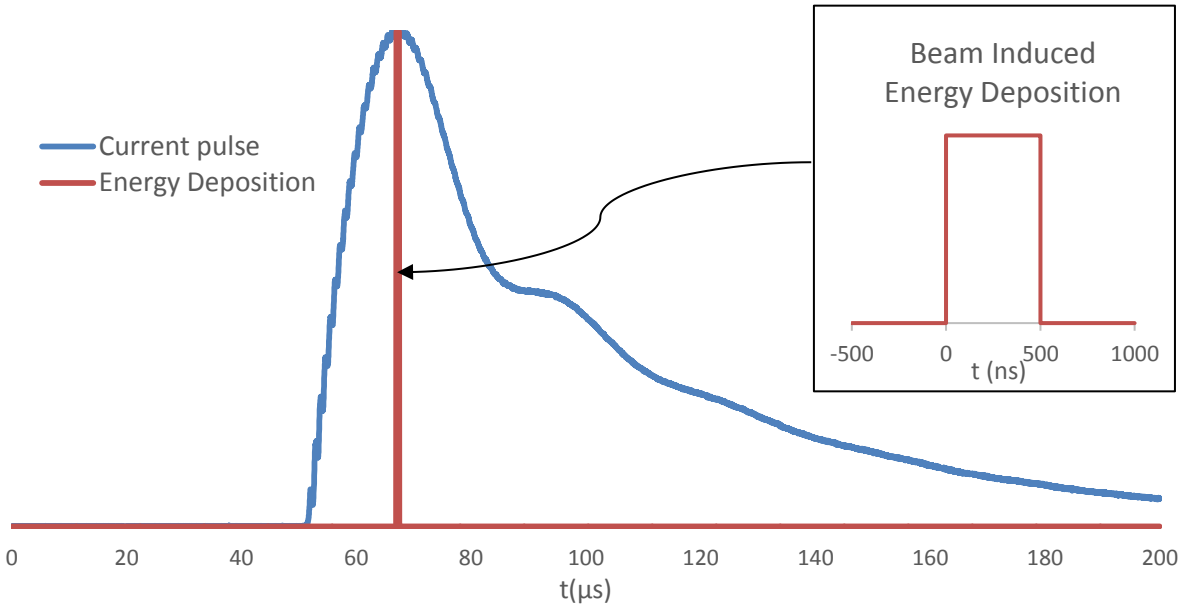

Figure 17 Current pulse and beam pulse superposition in time

Including both thermal loads into a thermal analysis requires the use of APDL commands, as two different heat generations can't be included with the basic tools provided by ANSYS® Workbench, because one imported heat generation would overwrite the other, instead of both

summing up. Then, the idea is to create an APDL code to store into tables the heat generation values of the current and beam pulse for each element, sum both of them up, and re-apply the total heat generated to each element of the model.

The procedure to apply both thermal loads in ANSYS through APDL coding is described in Annex A.2.

Then, it is possible to obtain the temperature evolution during the current pulse by performing a transient thermal analysis lasting 200 µs. The effect of including the beam energy deposition can be clearly observed, since there is a sudden increase of the temperature corresponding to the moment where the beam arrives on target and the secondary particles generated deposit their energy into the horn; in this case the maximum temperature reaches around 40°C after 200 µs (Fig.18).

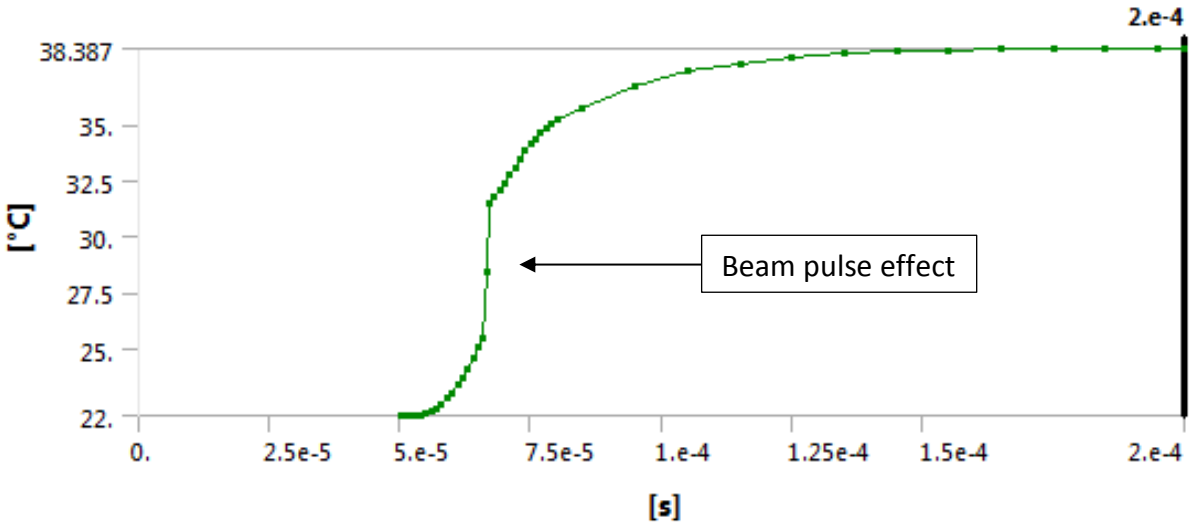

Figure 18 Maximum temperature evolution in the inner conductor

Since the time range of this analysis is very small, the convection and conduction effects won't have a significant influence in the temperature results in this case. The temperature distribution in the horn at the end of the current pulse shows that the maximum temperatures are located in the neck of the horn (Fig.19).

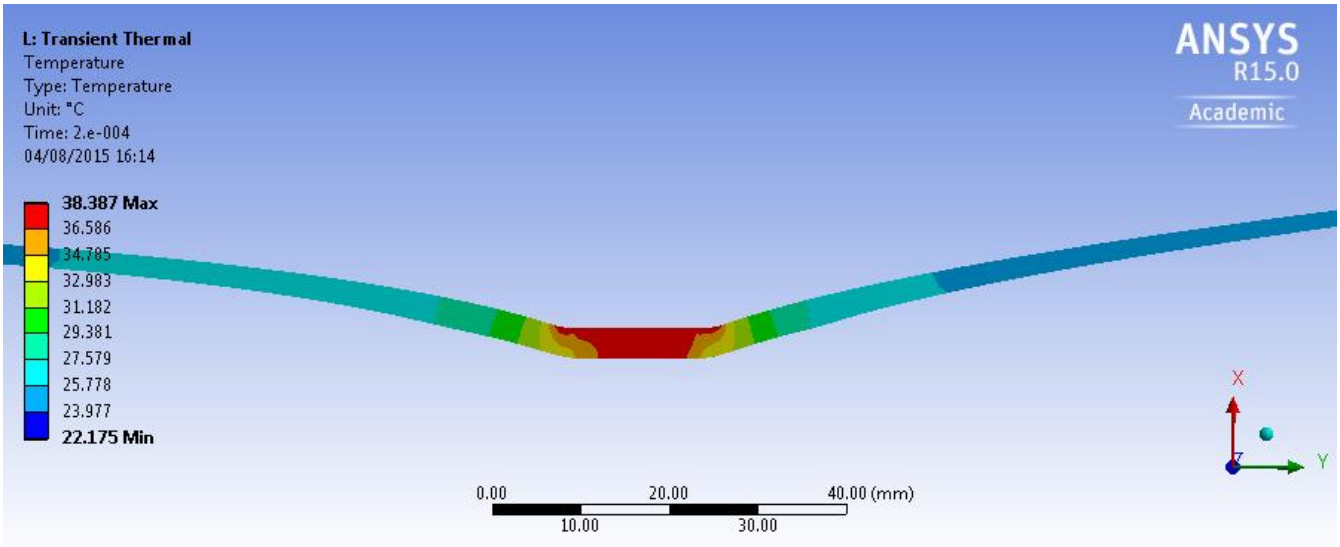

Figure 19 Temperature distribution in the inner conductor, current pulse + beam energy

In this case both Joule heat and beam energy deposition effects can be observed, since high temperatures are found in the edges of the neck in the external surface of the inner conductor, which corresponds to the effect of the Joule heating; and also in the whole central part of the horn neck, which is a consequence of the secondary particles interaction with the horn.

6.2 Steady-state thermal analysis

The temperature increase in the inner conductor depends strongly on the beam parameters considered for the analysis. The repetition rate, the number of pulses in each cycle and the length of the cycle are influencing the temperatures reached in the horn. The steady-state thermal analysis allows to calculate the mean temperature distribution after many cycles, once the temperature is stabilized.

As an example, we can consider the present beam parameters of the AD [4], with one single pulse per cycle, each cycle repeated after 90 seconds. In the end of the first cycle, the maximum temperature in the horn is 26°C, higher than the initial 22°C, which means that the maximum temperature reached after the second pulse will be even higher (Fig.20). For that reason, the convergence of the temperature evolution must be obtained, and a steady-state thermal analysis is performed with that purpose.

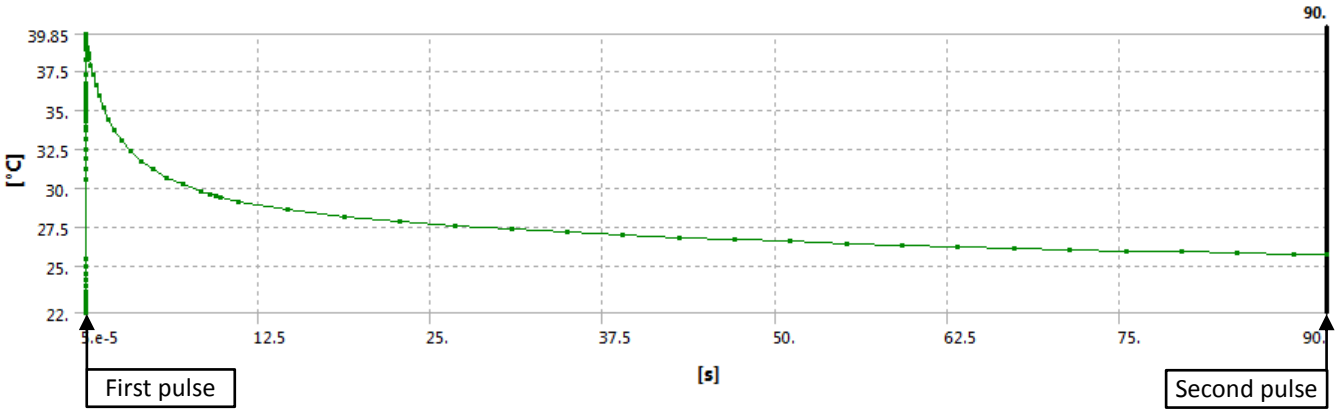

Figure 20 Maximum temperature evolution during one cycle of the "baseline" configuration.

6.2.1 Convection

For the steady state calculation it is important to consider convection effects, as the temperatures in the horn will decrease after each pulse thanks to heat transfer mechanisms. In a first approach, only the convection in the surfaces of the inner conductor is taken into account, and in a further analysis we include the conduction through the outer conductor. In this way, starting values for the temperature reached in the inner conductor are obtained, and the difference between considering or not the conduction through the outer conductor can be observed in a later stage.

The heat convection coefficient applied has to be chosen taking into account that the horn is air-cooled, the air is passing between the horn and the outer housing tube at the flow rate of 15 m^3/h. For this first approach, the convection coefficients applied will be 10 W/m^2K in the air-cooled volume, between the inner and the outer conductor, and 1 W/m^2K inside the inner surface of the horn, this value taken as natural convection but considering that, the access of air flow inside the horn is hampered by the outer conductor structure. The cooling parameters are described in Table 2.

Table 2 – Horn air-cooling parameters and heat convection coefficient considered

Air flow rate	Air pressure	Natural convection coefficient	Air cooling convection coefficient
15 m^3/h	4 bar	1 W/m^2K	10 W/m^2K

However, these heat convection coefficient values are quite conservative, and in order to obtain a more accurate simulation of the convection, in the future it will be necessary to perform a full CFD analysis to simulate the inner conductor behaviour under forced air cooling.

6.2.2 Considerations and APDL Code

The steady-state analysis takes into account the thermal boundary conditions, which is the convection in this case, and the total energy generated in the horn through a whole cycle. This energy depends on the number of pulses in each cycle, then it will be different for every set of beam parameters. As a first step, we will obtain the total energy generated in each element during one single pulse.

This total energy corresponds to the sum of the total energy deposition of the beam pulse, and the total Joule heat generated by the current pulse. The energy deposition values for each element in W/mm^3 have already been obtained previously, and the beam pulse has been approximated as a 500 ns stepped pulse as before. Therefore, the total energy deposition in each element corresponding to the beam pulse in J/mm^3 can be calculated by multiplying the values stored in the text file by 500 ns (Fig.21).

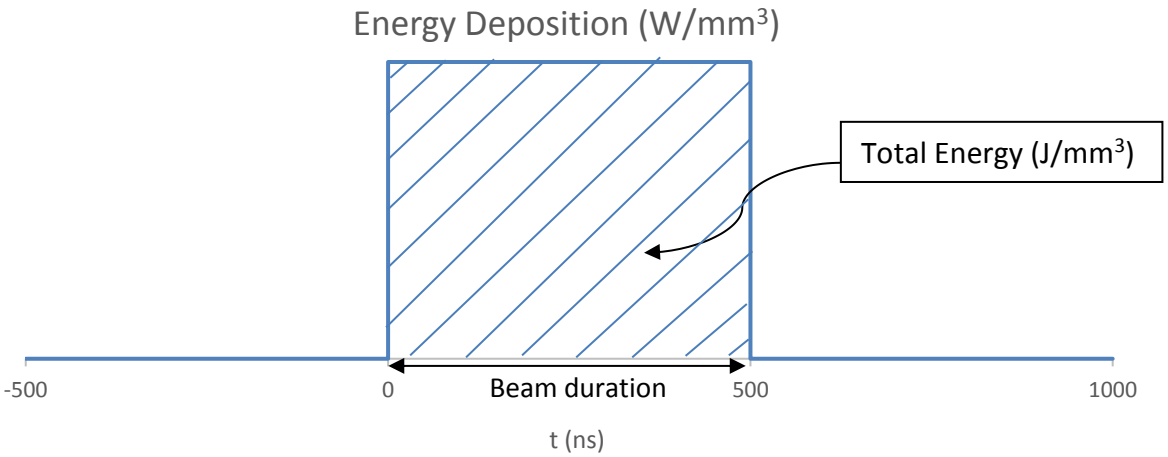

Figure 21 Total energy generated by the beam during one pulse

Concerning the total energy generated by the current pulse, the accurate procedure would be integrating the obtained Joule heating evolution with the time over the pulse length. We approximate this evolution with a triangular shape of 40 μs duration and as maximum value we will use the Joule heat values of each element at the time of maximum, stored in tables in the previous analysis (Fig. 22).

Thus, the total energy generated by the current pulse can be calculated by integrating the triangular approximation of the Joule heating over the 200 μs of the pulse, which means multiplying the Joule heating at the time of maximum by 20 μs.

At this point, we are able to obtain the total heat generated by the current flow and the beam interaction in one pulse. The energy generation input for the steady-state thermal analysis is the total energy generated by all the pulses distributed over the whole cycle duration.

This is equivalent to the energy generated in one pulse multiplied by the number of pulses and divided by the length of the considered AD super cycle (which includes 1, 5 or 10 pulses and a cooling phase). These operations are performed with the help of APDL commands included in the code used to apply the energy to all the elements of the model (Annex A.3).

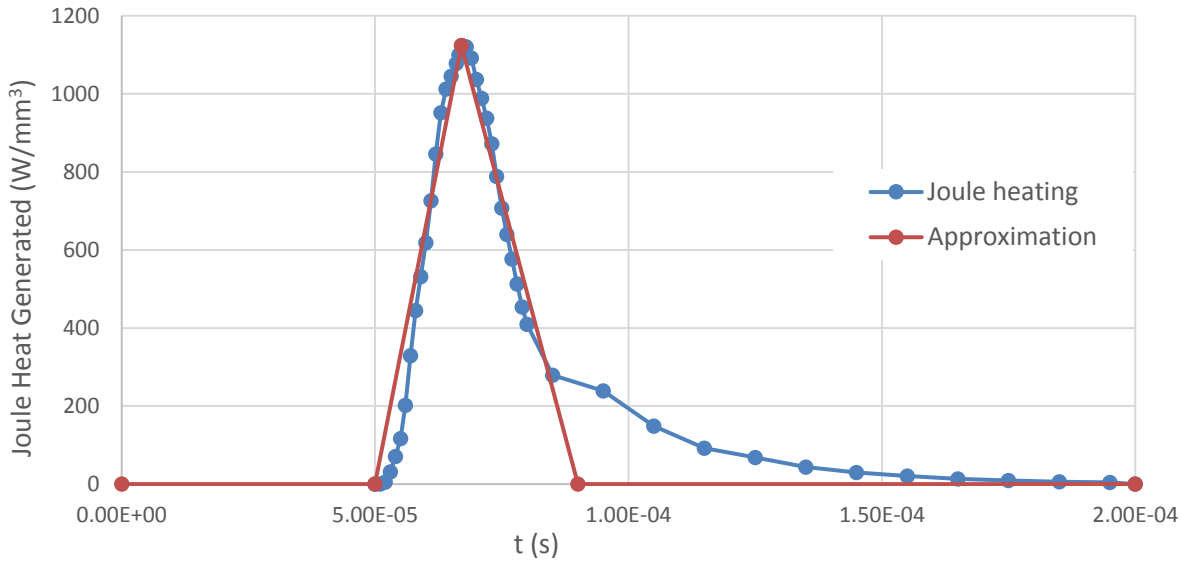

Figure 22 Joule heating approximation with a triangular shape

Following this procedure, the steady-state thermal analysis can be performed for the different operational scenarios as in [4]. As a result we obtain an approximation of the temperature distribution after the system will reach thermal equilibrium. By coupling the steady-state analysis with a transient thermal one, the obtained temperature distribution of the steady state calculation is considered as initial temperature in the transient analysis, and it's possible to calculate the maximum temperature reached in the inner conductor.

6.3 Full thermal analysis: beam parameters

In this section, full thermal analysis are carried out considering three different sets of beam parameters: baseline, accumulation and maximum accumulation mode [4]. This modes correspond to the present and possible future beam parameters implemented in the AD-Target area, and also supplementary simulations for the horn operation in the test bench will be performed.

6.3.1 Baseline mode

This is the present mode of operation, with one pulse per cycle at $1.5*10^{13}$ p/pulse, the cycle lasting 90 seconds. The temperature distribution obtained from the steady-state analysis results show that the highest temperatures are found in the central part and narrow end of the horn, with a maximum of around 35°C (Fig. 23).

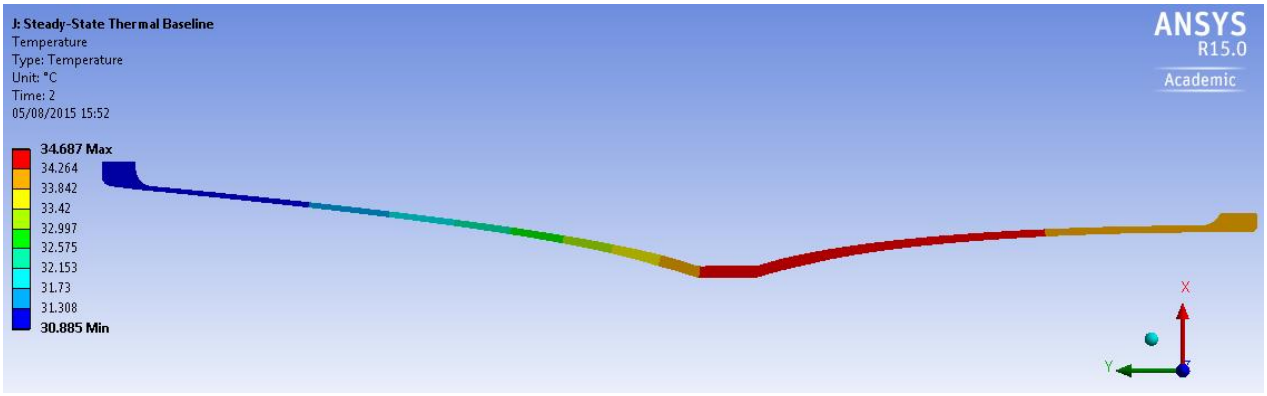

Figure 23 Temperature distribution after the steady-state analysis, baseline mode

With the heat convection values applied to the inner conductor in the present case, more heat is dissipated in the parabolic part of the horn than in the elliptical one, which explains why the narrow end of the horn reaches also high temperatures, as high as in the neck. However, it is expected that with more accurate heat convection coefficient values and the consideration of the heat conduction through the outer box of the horn, the temperature distribution will reach its higher values only in the neck of the inner conductor.

This distribution is used as initial temperature in a transient thermal analysis, where the thermal loads (energy deposition from the beam and Joule heating) are applied with an APDL code similar to the one used for the transient analysis lasting 200 µs, but in this case using a DO-loop to repeat the pulse each 90 seconds and reproduce a few cycles.

The transient thermal analysis results show that the maximum temperatures reached in the inner conductor after stabilization are around 55°C and located in the neck of the horn (Fig.24).

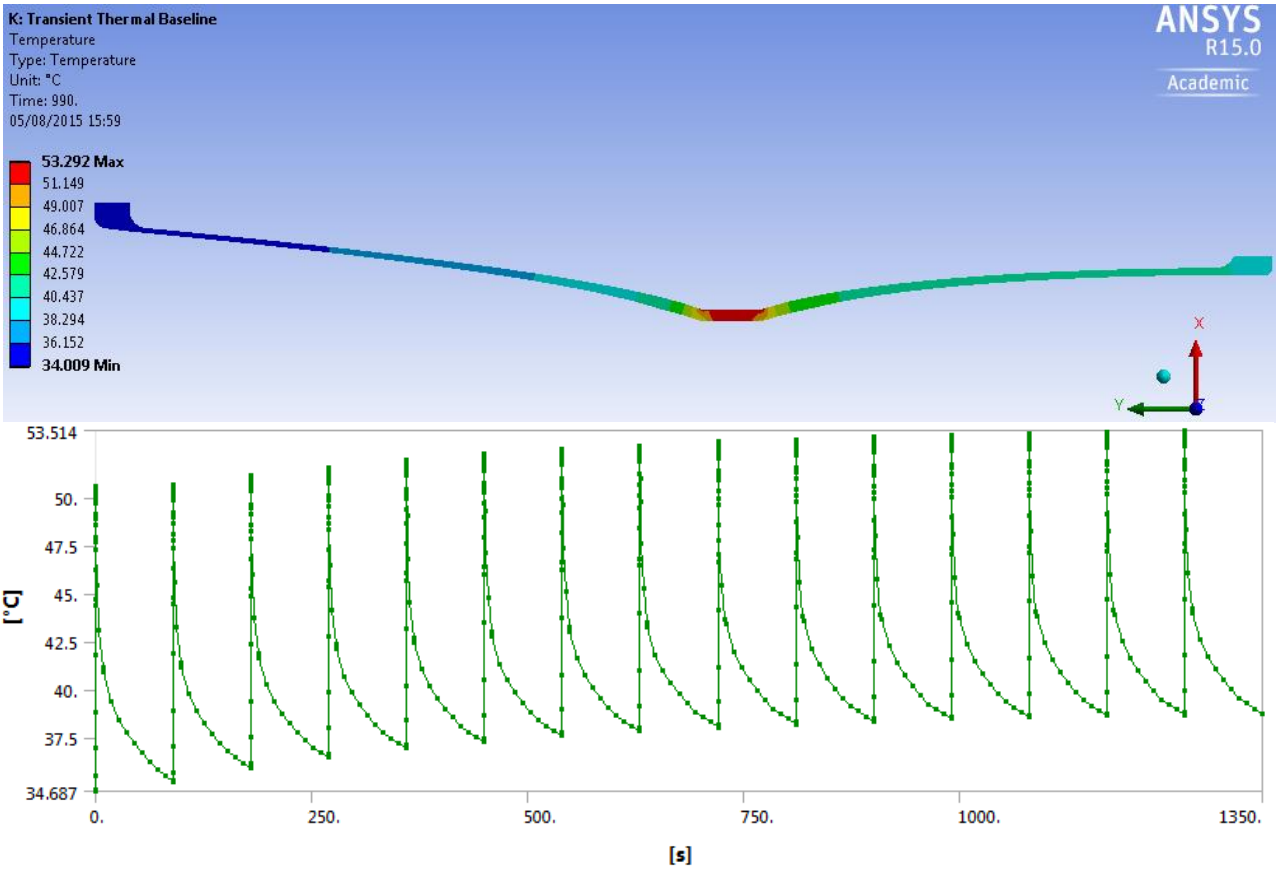

Figure 24 Temperature evolution and distribution, baseline mode

6.3.2 Accumulation mode

In this case, there are 5 pulses per cycle, one pulse each 15.6 seconds and the duration of the cycle is 148 seconds. It is possible to see that after 10 cycles the temperature is stabilized (Fig.25).

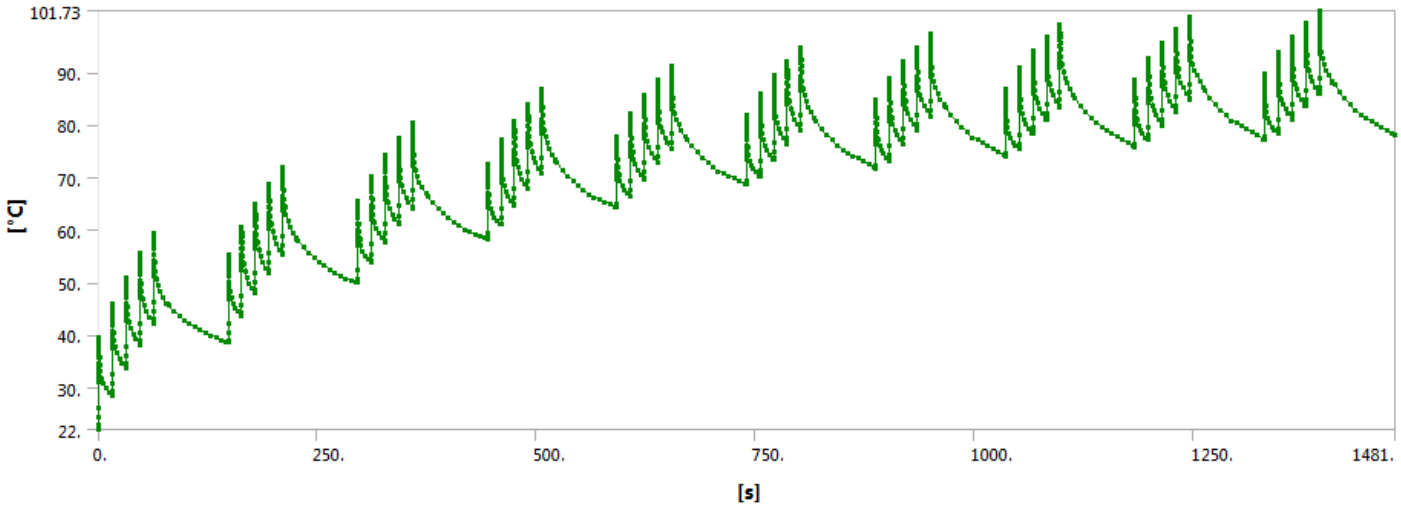

Figure 25 Temperature evolution in the inner conductor during 10 cycles, accumulation mode

The maximum temperature reached would be around 100°C**,** which is not acceptable from the point of view of the horn material properties, as the nominal service temperature of the AA7075 is between 80°C and 100°C. In fact, many properties of this alloy drop at high temperatures, which is the case of the tensile yield strength for example, which is high at room temperature but suffers a sharp fall at 100°C (Fig.26).

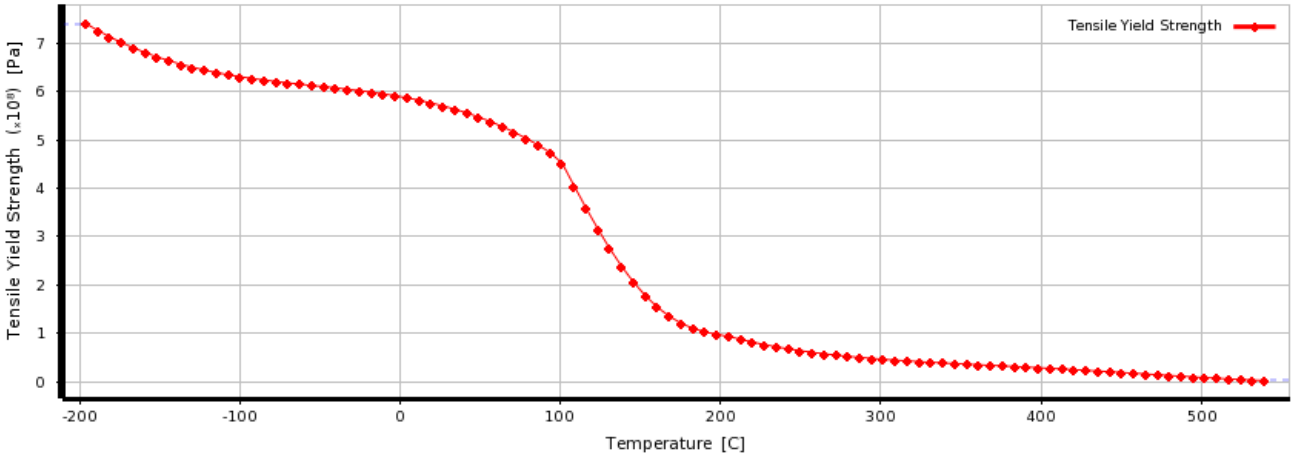

Figure 26 AA7075-T6 Tensile yield strength evolution with temperature, data imported from the Material Properties Database (MPDB) software [5]

6.3.3 Maximum accumulation mode

For the maximum accumulation mode the beam parameters are 10 pulses per cycle, one each 9.6 seconds and 166 seconds as cycle length. Performing the steady-state analysis with this parameters reveals that the convergence temperature after the steady state is already higher than the maximum service temperature (90°C) (Fig.27), and in the subsequent transient thermal

analysis it can be seen that the maximum temperature reached is beyond the acceptable temperature limits in the horn (140°C) (Fig.28).

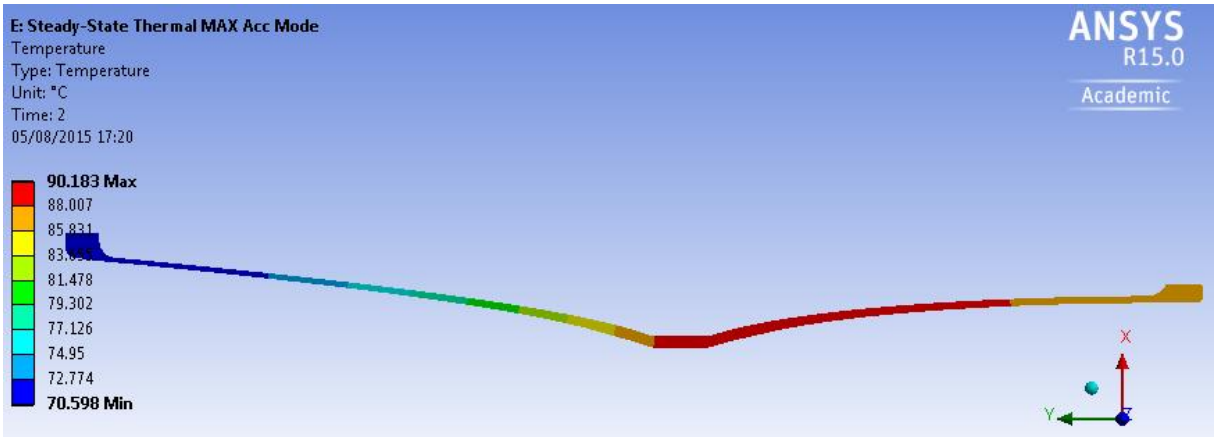

Figure 27 Steady-state analysis temperature distribution, maximum accumulation mode

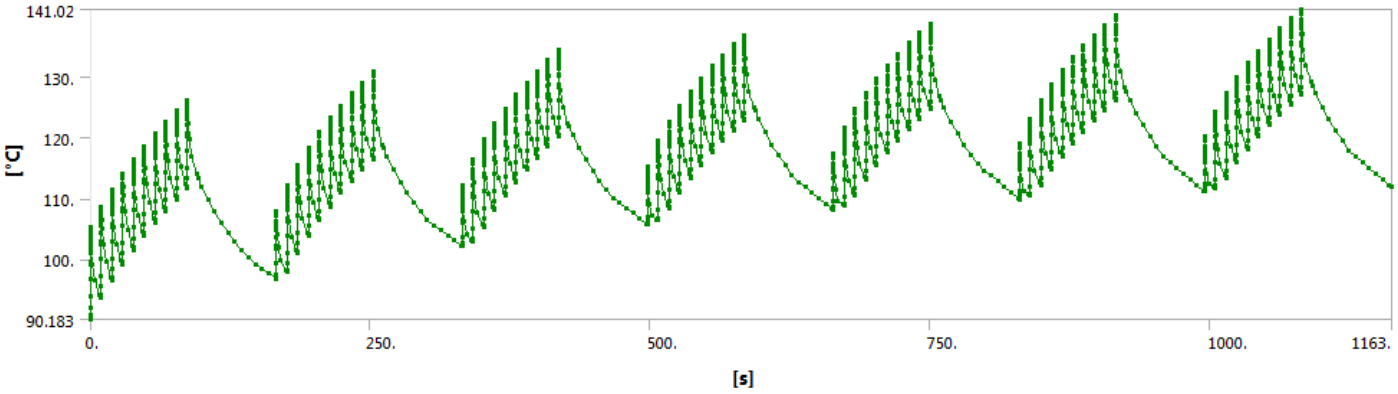

Figure 28 Temperature evolution, maximum accumulation mode

The results obtained are not acceptable for the accumulation modes, as the maximum temperatures reached exceed the limits of the service temperature. For that reason, it is necessary to verify the boundary conditions applied to the model, as for example considering the conduction through the outer housing. Since the convection effects will be determined through CFD-simulations that will be carried out in the future, the heat convection coefficient values will remain the same for the conclusion of this paper despite being highly conservative.

6.3.4 Outer conductor modelling

In order to simulate the behaviour of the temperature in the inner conductor when the conduction through the outer elements is considered, a similar model is built in order to reproduce the geometry of the external housing (Fig.29).

The axisymmetric geometry of the model is also taken into account in this case, and the current and ground voltage excitations are applied through the strip-line and the outer box respectively (Fig. 30), both being separated by a vetronite insulation layer**.**

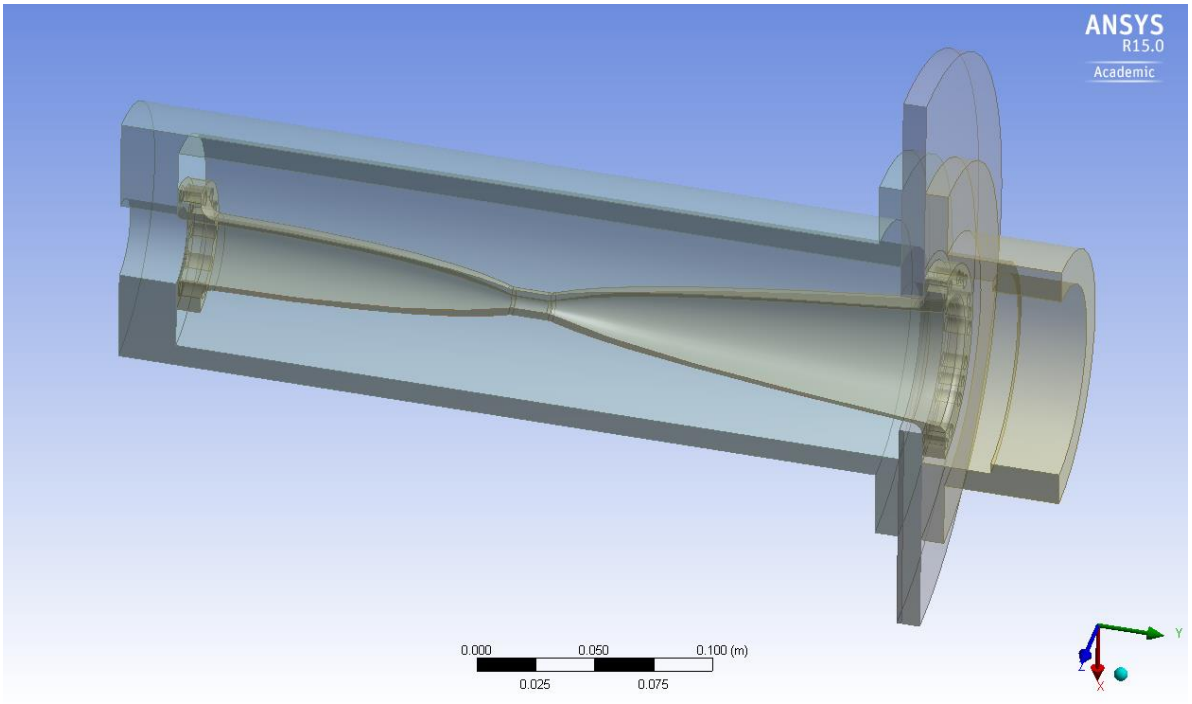

Figure 29 External conductor modelled with help of ANSYS® Design Modeler [8]

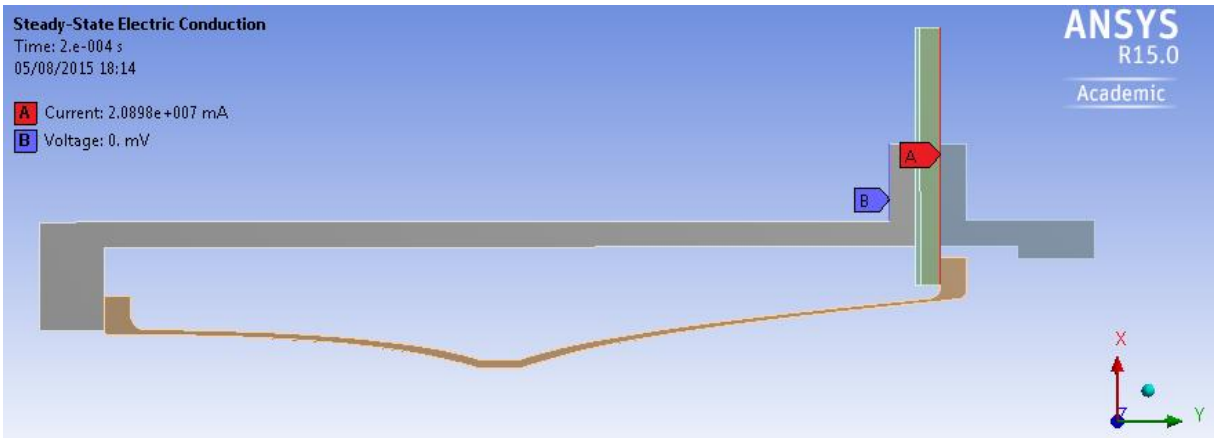

Figure 30 Electrical excitations in the horn+outer conductor model

The procedure for the electrical and thermal analysis with this model is exactly the same as considering only the inner conductor. The electrical analysis results are comparable to the ones obtained in the inner conductor itself, with the highest values of Joule heating located in the outer edges of the horn neck.

The results obtained after the steady-state analysis and posterior transient thermal analysis are positive in terms of maximum temperature in the baseline (47°C) and accumulation mode (75°C), but the temperatures appear to be still too high for the maximum accumulation mode (103°C) (Fig. 31).

a) Baseline

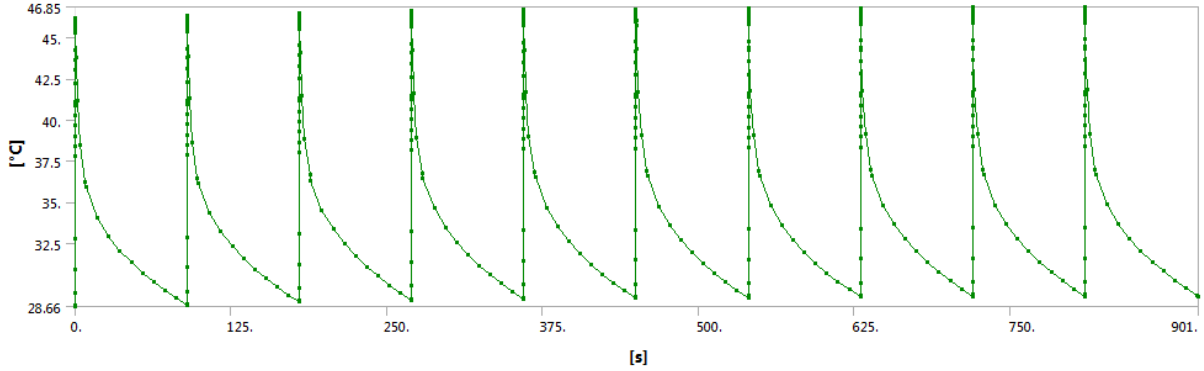

b) Accumulation mode

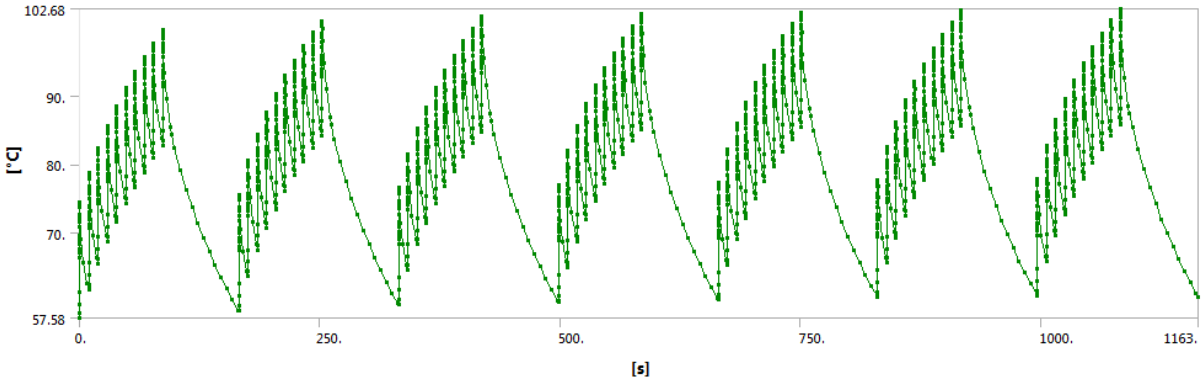

c) Maximum accumulation mode

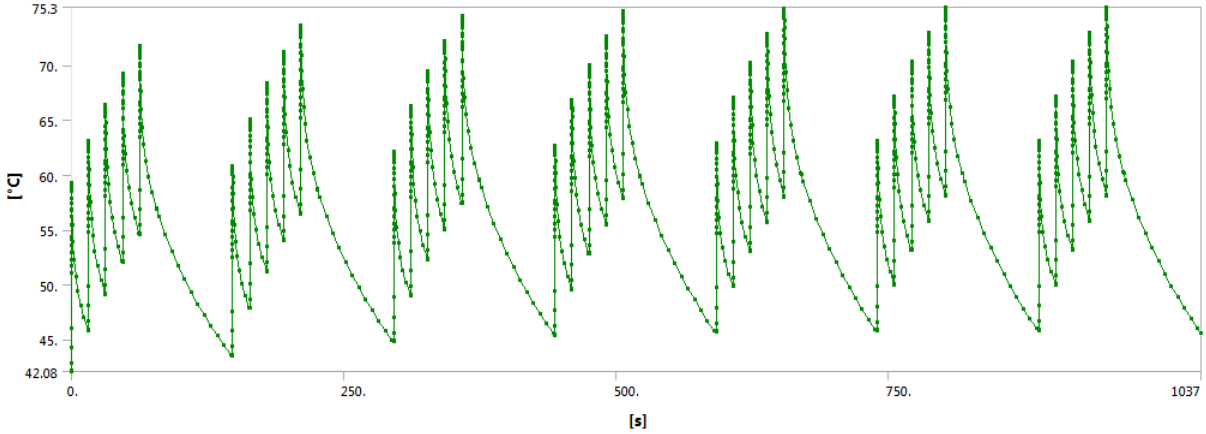

Figure 31 Temperature evolution after stabilization for different beam parameters, horn and external conductor considered

It is necessary to point out that the contacts between the inner conductor and the outer housing parts have been defined as *bonded*, and thus the heat conduction between both parts is considered as perfect, without heat losses. This is a very optimistic approach, and the conduction coefficient between the inner and outer conductor must be evaluated in the future in order to obtain more accurate results.

6.3.5 Test bench operation

The magnetic horn will be tested at 400 kA under high repetition rates to simulate the operation in the AD-Target area during a long period and identify the possible failures due to thermal and structural stresses. In order to reproduce the thermal behaviour of the horn in the test bench, a transient thermal analysis has been carried out using the horn model (including the outer conductor), considering only the Joule heating produced by the current pulse.

A repetition rate of 9.6 seconds was first considered, and as the results after 50 cycles were positive and the maximum reached temperature once stabilized was acceptable (75°C), a higher repetition rate of 4.8 seconds was applied, obtaining too high temperatures in this case after 100 cycles (115°C) (Fig. 32).

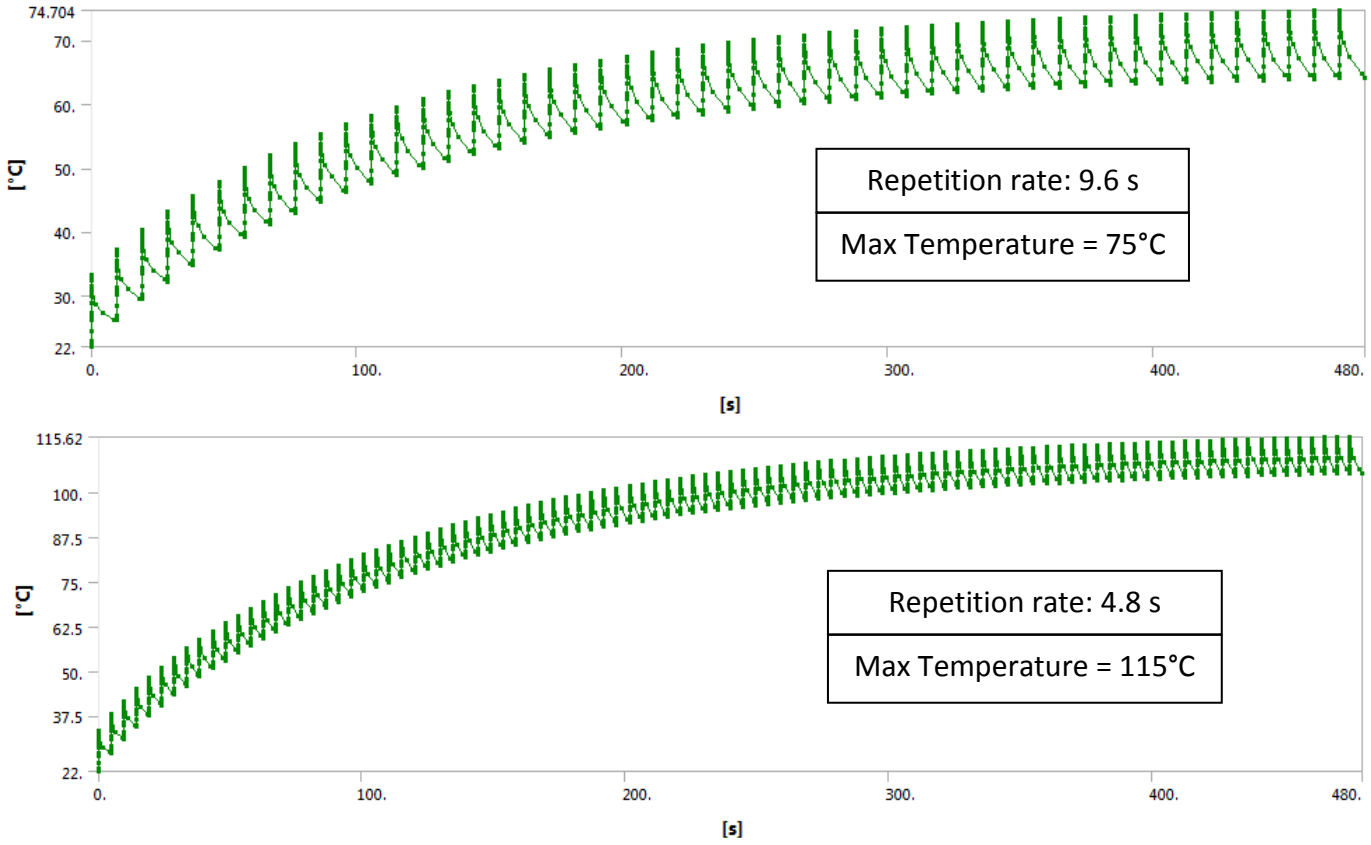

Figure 32 Temperature evolution for different repetition rates in the test bench conditions

6.4 Full thermal analysis conclusions

The main outcome of this section is the development of the procedure to perform thermal simulations in the AD horn by including the effects of the current pulse and the beam interaction with the horn, and analysing the thermal behaviour throughout the time under different beam parameters.

Since the boundary conditions such as convection and conduction have to be reviewed by further studies in the future, the results of the thermal simulations carried out are not final. However, thanks to the obtained results we can have an idea of the influence of these boundary conditions in the evolution of the temperatures reached in the magnetic horn, and how the beam parameters will affect the maximum temperatures attained.

7. Structural Analysis of the AD Horn

7.1 Electromagnetic Forces

The electromagnetic forces generated by the current pulse are the origin of high structural stresses that need to be considered in this study. Due to the skin effect, we can consider that the current is concentrated in the outer layer of the inner conductor, the skin depth evaluated being less than the half of the wall thickness of the horn in its thinnest part as in Ref. [1].

Therefore, the electromagnetic force will be modelled in this analysis as an external pressure applied to the outer layer of the inner conductor. Given the sense and direction of the electric and magnetic fields, this pressure is compressive and perpendicular to the outer surface. The pressure values can be calculated according to the approximate formula [1]:

$$B = \frac{\mu_0 I}{2\pi R} \; ; \; p = \frac{B^2}{2\mu_0},$$

with $I[A]$, $\mu_0 = 4\pi \cdot 10^{-7}[H/m]$, $p[Pa]$ and $R[m]$ the horn outer radius. The external pressure in the horn is then space- and time-dependent, as the horn outer radius changes along the horn Y-coordinate and the current pulse varies along the time.

7.2 Static Structural Analysis

The main purpose of this analysis is to evaluate the static stresses in the horn under peak electromagnetic forces. Based on the horn technical drawings, the outer radius values are obtained in function of the Y-coordinates of the horn, and taking into account the formulas previously presented, we are able to calculate the pressure corresponding to the maximum intensity (400 kA) along the horn surface.

This pressure can be applied as *tabular data* in a static structural analysis, considering a different pressure for each Y-coordinate of the outer layer of the horn (Fig.33). The pressure values vary from 2.8 MPa in the thin wide end to 60 MPa in the neck of the horn.

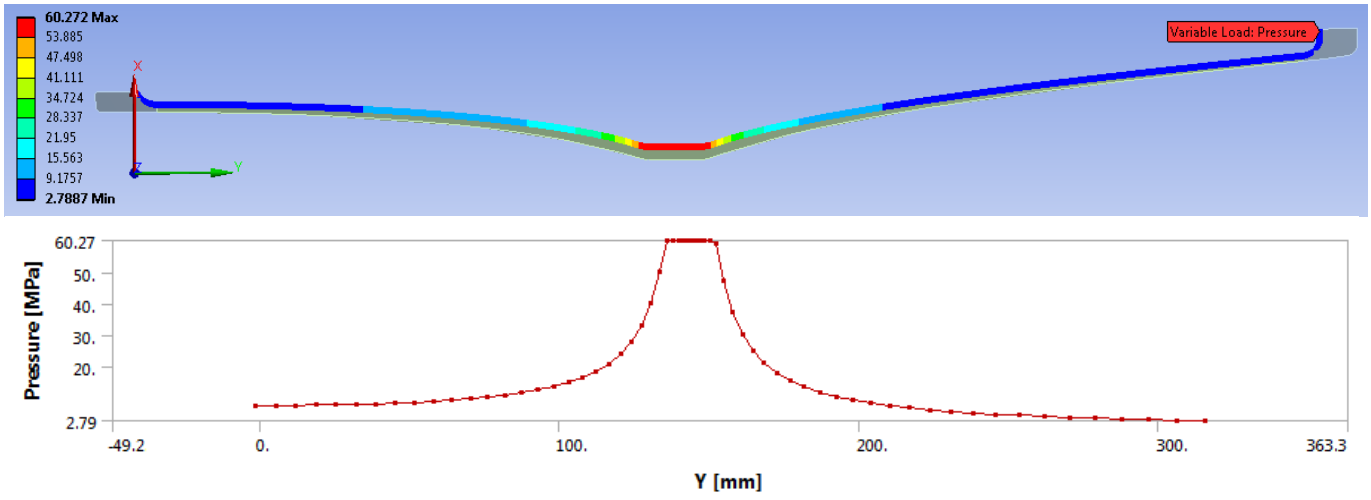

Figure 33 Maximum pressure applied along the length of the horn

As boundary conditions for this analysis, both horn ends have to be blocked longitudinally, modelled in the structural analysis as *fixed supports.*

The results of the static analysis show that the largest stresses are tensile in the circumferential direction (Z here), located in the inner surface of the central part of the neck the horn (Fig. 34), while also large compressive stresses are developed in the axial direction (Y), located in the edges of the neck of the horn, in the outer surface in this case (Fig.35). The origin considered is located as shown in Fig. 33, coincident with the origin used to specify the outer radius of the inner conductor in function of the Y-coordinates in the horn technical drawings [2].

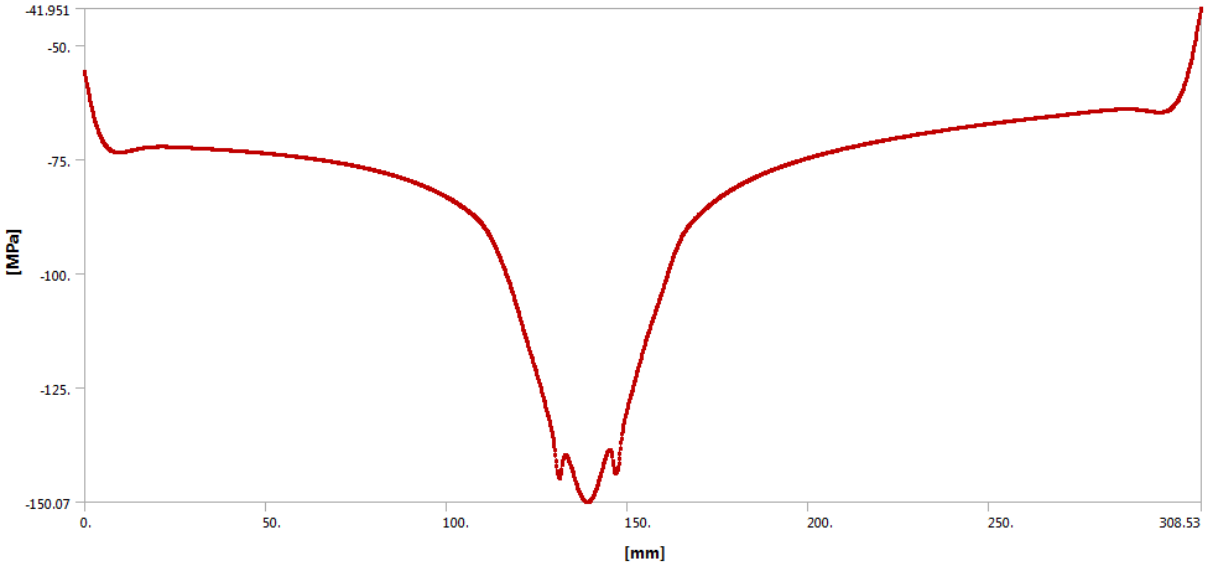

Figure 34 Compressive circumferential stresses along the horn inner surface

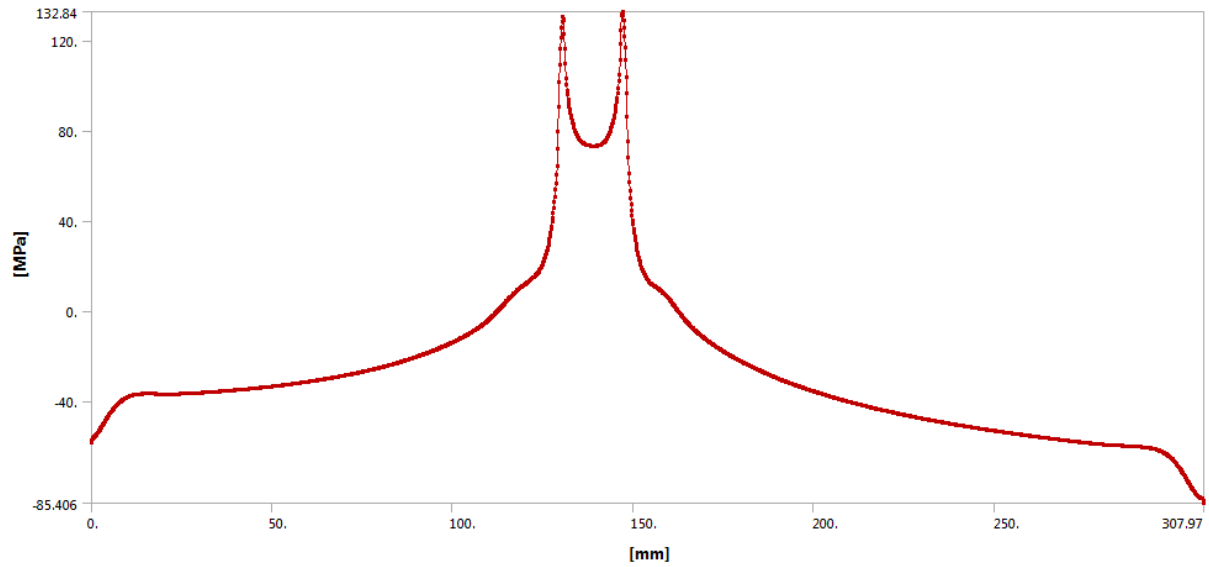

Figure 35 Tensile longitudinal stresses along the horn outer surface

The maximum Von Mises stress is 204 MPa in the inner surface of the neck of the horn (Fig.36), this level of stress is quite acceptable considering that the yield strength of the aluminium alloy is around 430-450 MPa and the typical safety factor required with respect to yield strength is 1.6.

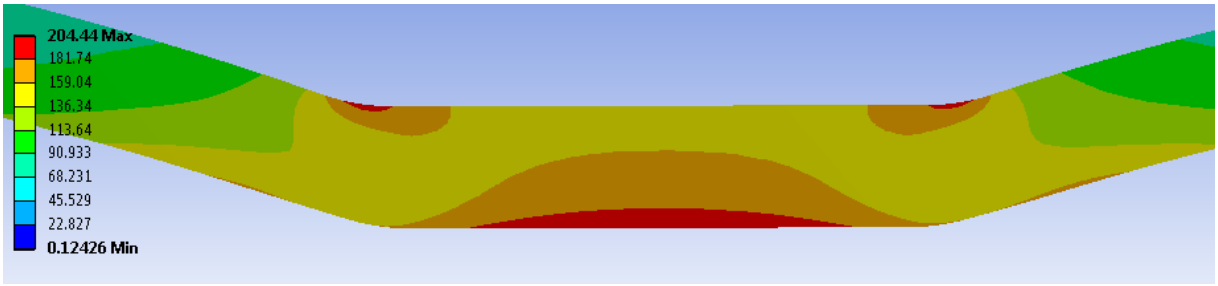

Figure 36 Maximum Von Mises stress distribution in the horn in MPa

The main displacements obtained after the static analysis are in the axial direction and of the order of 60 µm (Fig.37).

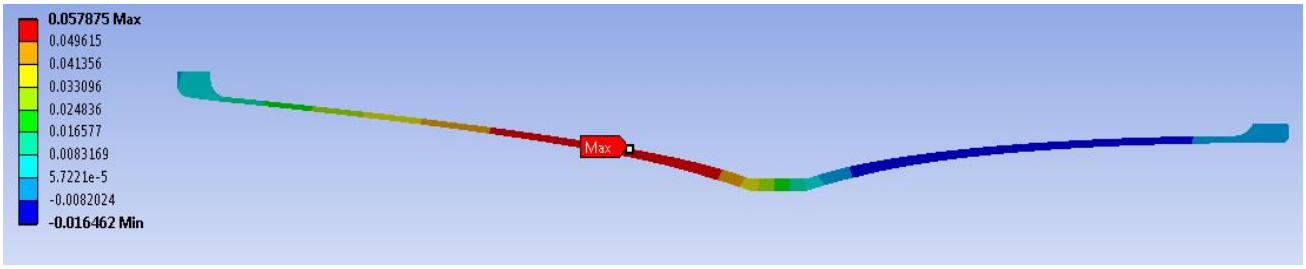

Figure 37 Axial displacements in the horn under peak electromagnetic forces in mm

The range of stresses and displacements for the axisymmetric model are presented below in Table 3.

Table 3 – Range of displacements and stresses in the horn under peak electromagnetic forces

Range of Displacements [mm]		
Radial (X)	Max	0.0008
	Min	-0.017
Axial (Y)	Max	0.058
	Min	-0.016
Range of Stresses [MPa]		
Radial (X)	Max	34
	Min	-60
Longitudinal (Y)	Max	132
	Min	-86
Circumferential (Z)	Max	8
	Min	-150
Max Von Mises Stress		**204**

It is important to consider in this case the possibility that higher non-axisymmetric displacements and stresses exist and are not taken into account in the axisymmetric model. For that reason, we perform the same static structural analysis taking into account the whole model of the horn. The results of the static structural analysis performed in the whole model are of the same order and with very similar stress and displacement distributions than the ones obtained for the axisymmetric one (Fig.38).

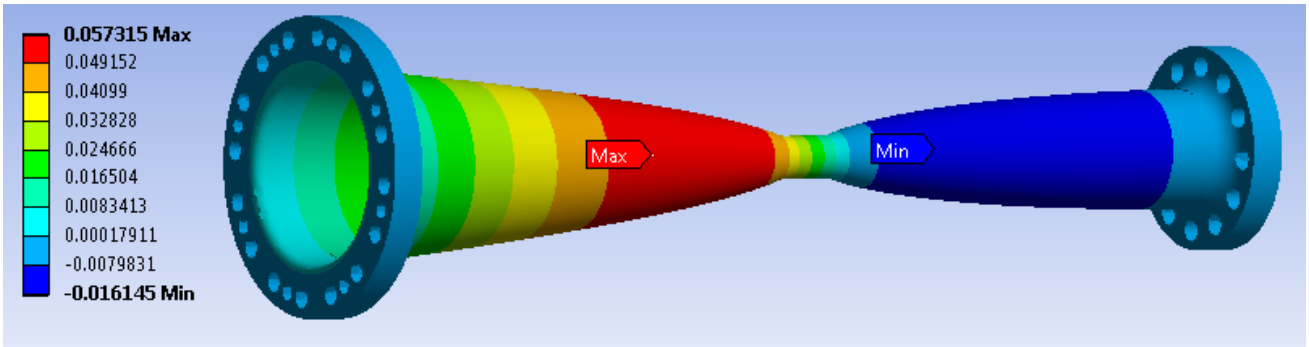

Figure 38 Axial displacements in the whole horn model under maximum pressure in mm

A buckling analysis has to be carried out as well in the whole tri-dimensional horn model, since the first modes of buckling are not axisymmetric and therefore can't be obtained with the reduced axisymmetric model. The buckling multiplicative factor obtained (**5.6**) is well above the range of safe values, typically of the order of 3.5-4.0. This buckling factor corresponds to the third circumferential mode of buckling, which is non-axisymmetric, as can be seen in Fig.39 (where a scale factor has been applied in order to appreciate better the deformation).

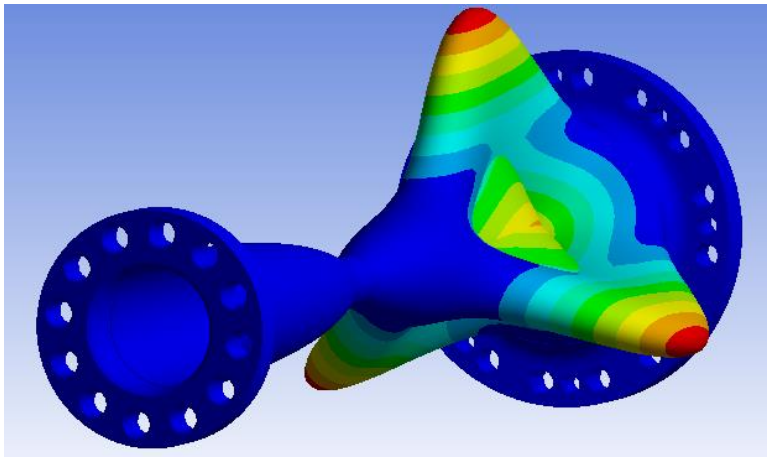

Figure 39 Third circumferential mode of buckling

7.3 Transient dynamic analysis

7.3.1 Analysis considerations

This analysis is performed in order to study the dynamic response of the horn under impulsive pressure loading. It is considered that the vibrations in the horn are damped from one pulse to the next one, therefore only single pulse loading is applied.

The natural frequencies of the horn can be previously obtained by performing a modal analysis. It is important to notice that, as we are considering the axisymmetric model, the obtained modes are only axisymmetric modes. Therefore, lower non-axisymmetric frequencies could be obtained by analysing the complete model of the horn. The lowest obtained frequencies for the axisymmetric model are f_{0m}= 8694, 14689, 23718, 29449… Hz.

The impulse of electromagnetic forces is applied as a triangular pulse of external pressure lasting 60 µs in order to approximate the pressure impulse generated by the current pulse. The maximum pressure applied in the triangular pulse corresponds to the maximum intensity, we use therefore the same pressure table than the one employed in the static analysis.

This pressure is imported from an *External Data* table, which is applied with a ramped loading at 3 different time-steps (10µs, 40µs and 70µs): by specifying different *Scale* values (0 or 1), the triangular pulse can be reproduced. The analysis runs until 1.25 ms in order to see the oscillations evolution (Fig. 40).

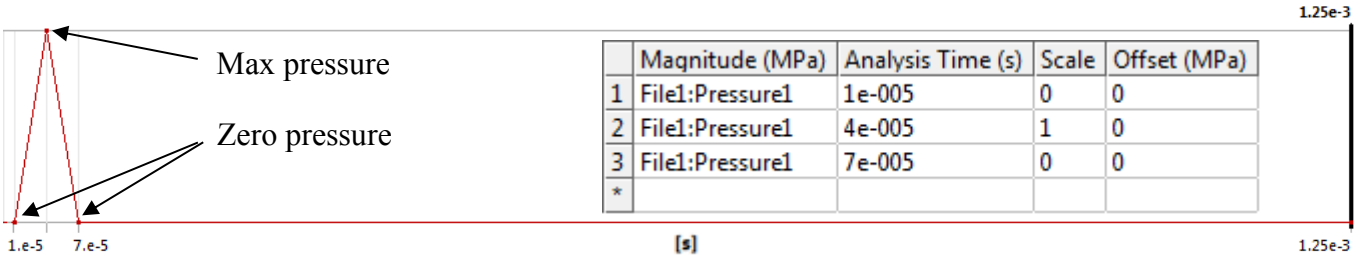

	Magnitude (MPa)	Analysis Time (s)	Scale	Offset (MPa)
1	File1:Pressure1	1e-005	0	0
2	File1:Pressure1	4e-005	1	0
3	File1:Pressure1	7e-005	0	0
*				

Figure 40 Triangular pulse of external pressure included in ANSYS® Transient Structural

7.3.2 Transient dynamic results

Similarly to the static analysis results, the maximum displacements are found in the axial direction (Fig.41), and are of the same order than the static ones (± 0.084 mm). Since no damping effects have been considered, the oscillations a attenuated after 1.25 ms, it is be necessary therefore to consider the supporting outer box at a later stage.

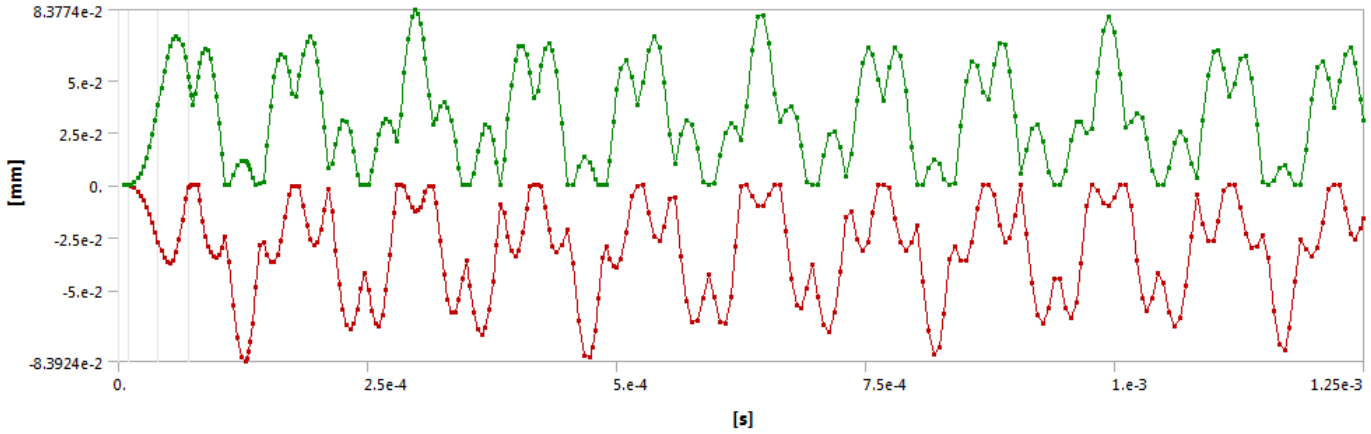

Figure 41 Minimum (red) and maximum (green) dynamic displacements in the axial direction

The maximum Von Mises equivalent stress is 212 MPa, very similar to the one obtained in the static analysis (Fig.42). The highest normal stresses are both located in the neck of the horn as previously, although the highest tensile stresses in the longitudinal direction (180 MPa) are in this case larger than the compressive circumferential stresses (around 150 MPa) (Fig.43).

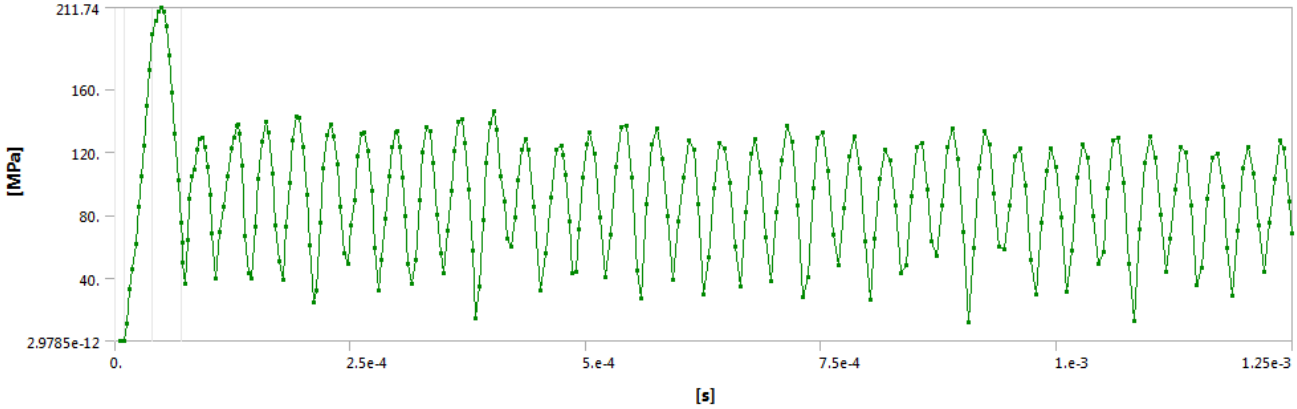

Figure 42 Maximum Von Mises equivalent stress, transient dynamic analysis

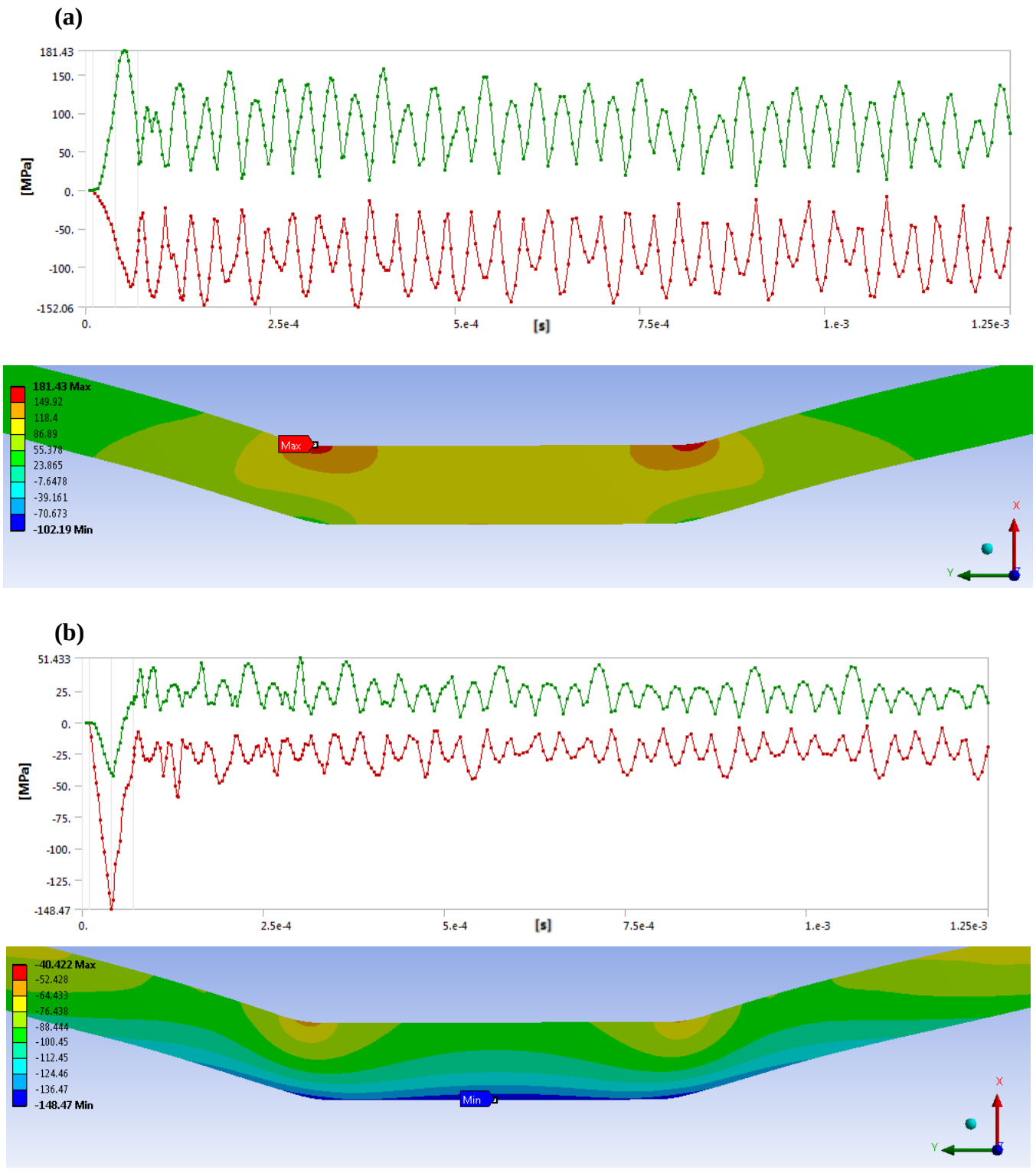

Figure 43 Longitudinal (a) and Circumferential (b) dynamic stresses in the horn in MPa

The range of stresses in the axial direction is negligible compared to the circumferential and longitudinal stresses. The maximum and minimum stresses and displacements in the different directions are given in Table 4, showing that the values obtained in the transient dynamic analysis are of the order of the static ones.

Table 4 – Range of displacements and stresses in the horn – dynamic analysis.

Range of Displacements [mm]		
Radial (X)	Max	0.013
	Min	-0.023
Axial (Y)	Max	0.084
	Min	-0.083
Range of Stresses [MPa]		
Radial (X)	Max	14
	Min	-60
Longitudinal (Y)	Max	181
	Min	-152
Circumferential (Z)	Max	51
	Min	-148
Max Von Mises Stress		**211**

The forced frequencies obtained in the dynamic analysis correspond with the natural frequencies found in the modal analysis. The lowest forced frequency is around 8.7 kHz, as obtained for the displacement oscillations in the axial direction for a specific node (Fig.44) and the next frequencies (15 kHz, 24 kHz,…) are also found in the radial displacement and normal stress oscillations (Fig.45).

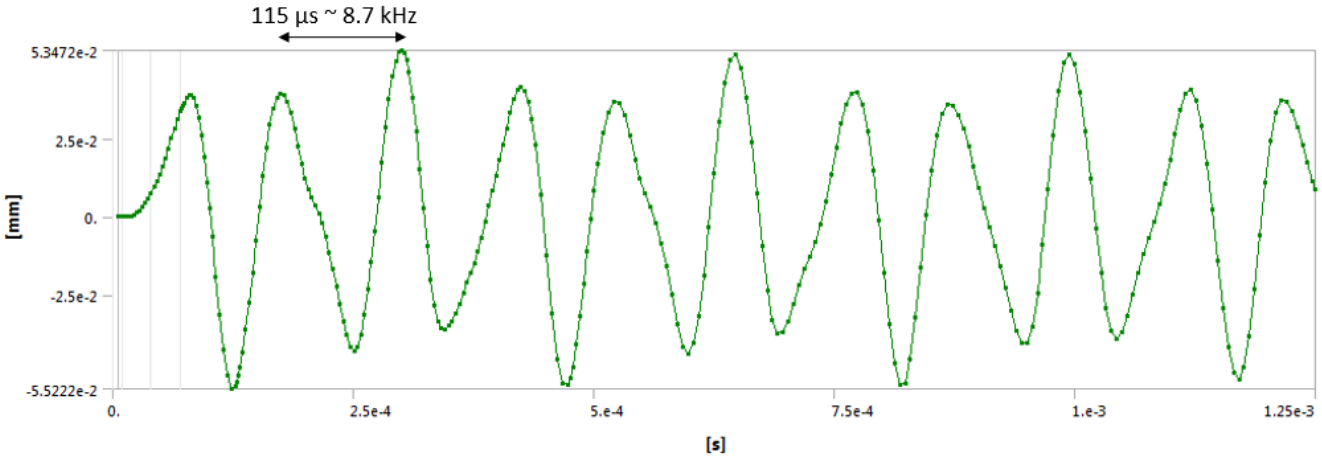

Figure 44 Maximum axial displacement of a specific node (central part of the horn)
Lowest forced frequency = 8.7 kHz

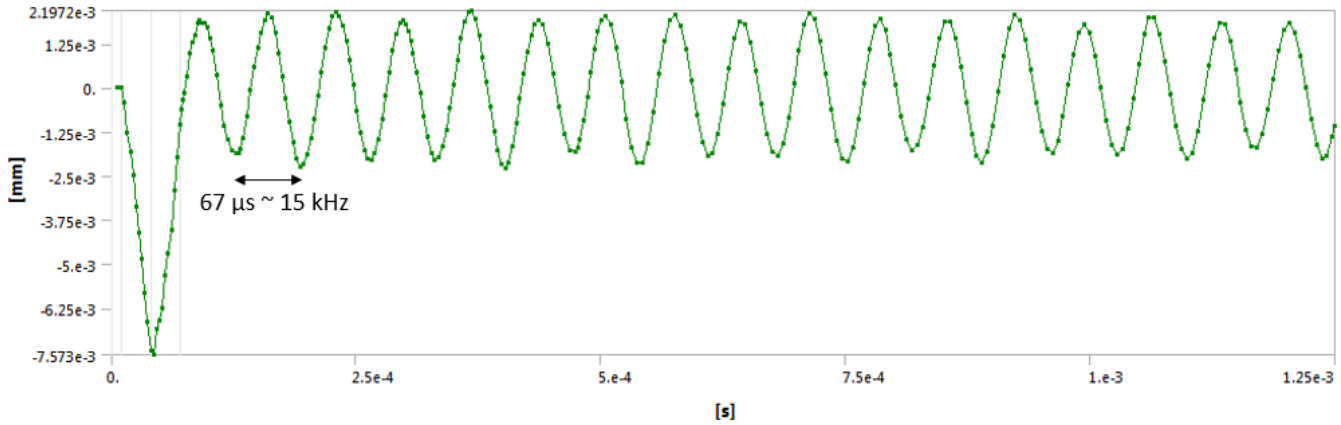

Figure 45 Maximum radial displacement of a specific node (central part of the horn)
Forced frequency = 15 kHz

7.3.3 Whole inner conductor model

The modal analysis performed previously calculates only the frequencies corresponding to the axisymmetric modes of deformation. It is necessary to consider the whole model in order to obtain all the deformation modes of the AD horn, and evaluate if there are lower frequencies corresponding to non-axisymmetric modes that should be taken into consideration.

The results of the modal analysis carried out in the whole horn model show much more natural frequencies than the axisymmetric one, also lower than 8 kHz, as shown in Fig.46. These modes correspond indeed to non-axisymmetric modes of deformation (Fig.47).

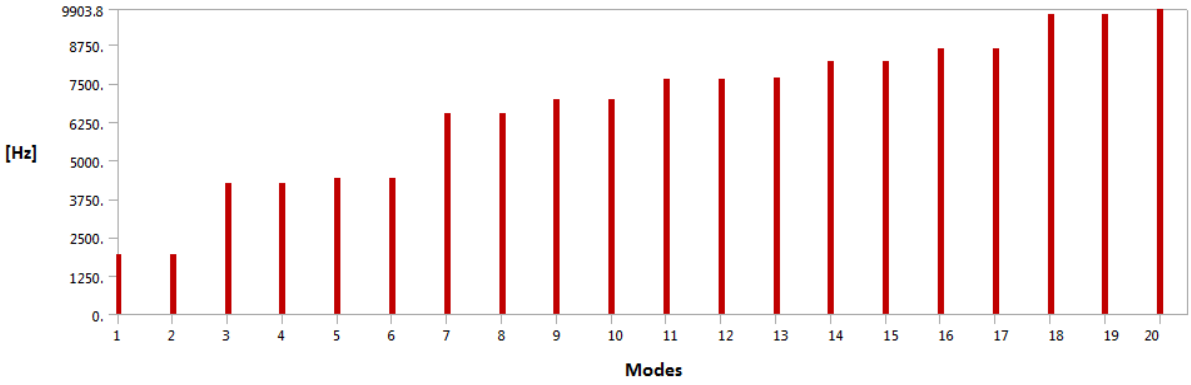

Figure 46 Natural frequencies in the whole inner conductor model

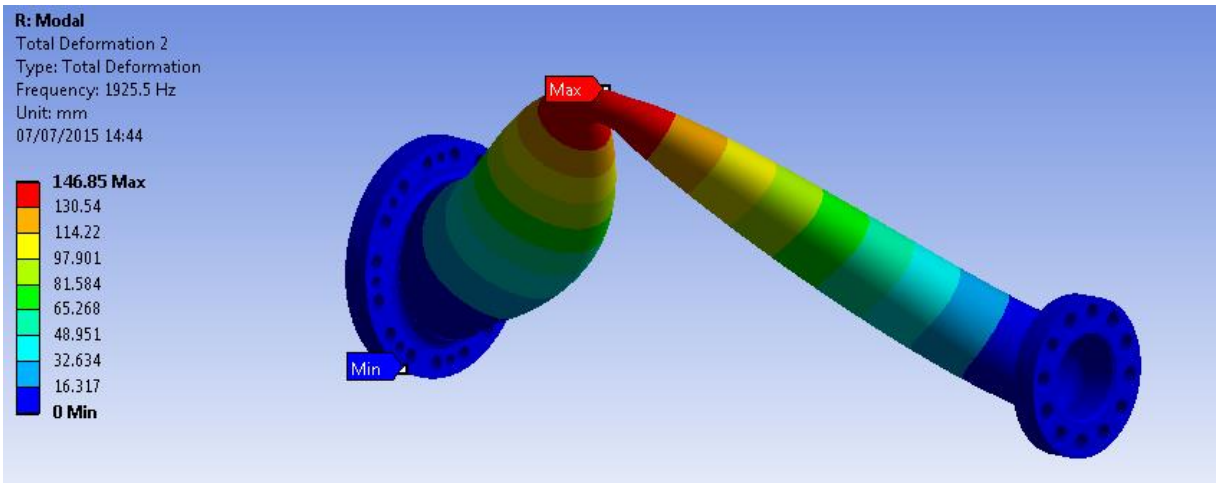

Figure 47 Non-axisymmetric deformation – Lowest natural frequency (2 kHz)

The results of stresses and displacements of the transient dynamic analysis performed in the whole inner conductor model are almost identical to the ones obtained for the axisymmetric model, as well as the lowest forced frequencies that are also found in the axial displacements and around 8 kHz (Fig.48).

Therefore, even if there are lower natural frequencies corresponding to non-axisymmetric modes, the lowest forced frequencies are the same than for the axisymmetric model, which will be used in the future because of its simplicity.

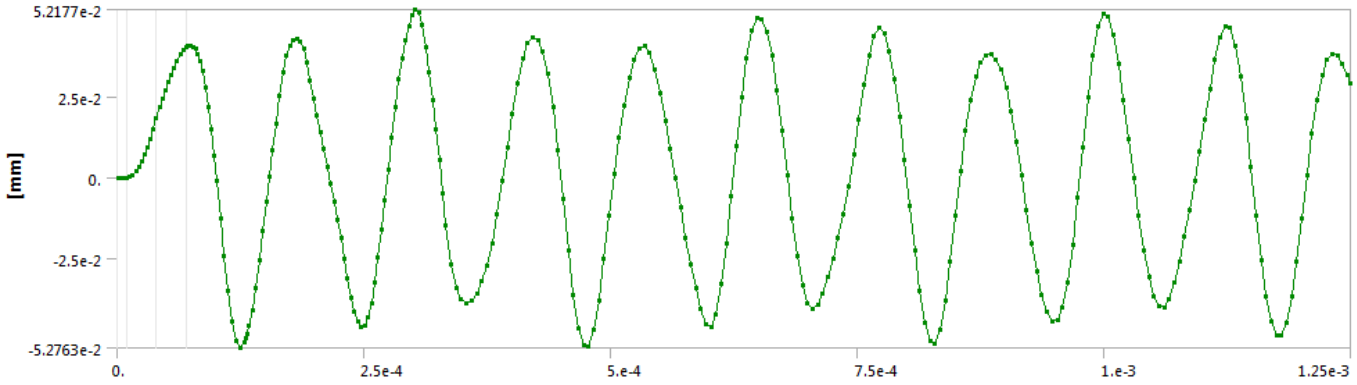

Figure 48 Maximum axial displacement of a specific node (central part of the horn)
Whole horn model – Lowest forced frequency = 8 kHz

7.3.4 Outer conductor consideration

The dynamic analysis is performed in this case including the external box of the horn modelled for the full thermal analysis. The contact between the inner conductor and the outer housing is set as *Bonded* and as boundary conditions for the analysis the strip-line and the horn outer support will be fixed elements (Fig.49).

As a first approach a static structural analysis is carried out, applying the pressure load corresponding to the current peak in the inner conductor by using *Tabular Data* as before. The results obtained are almost identical to the ones without the outer conductor, with maximum Von Mises equivalent stress values of around 205 MPa (Fig.50).

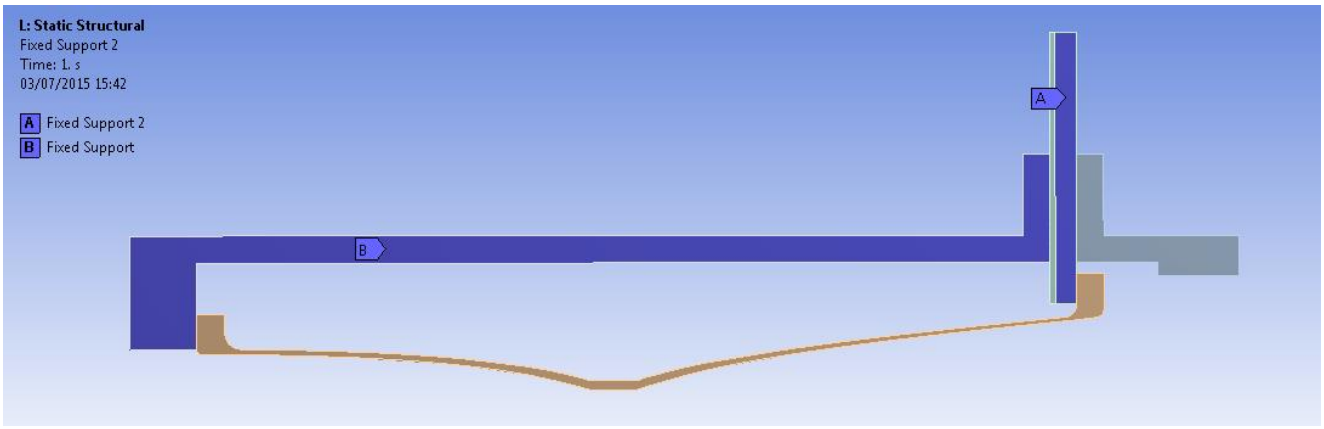

Figure 49 Fixed supports in the inner + outer conductor model

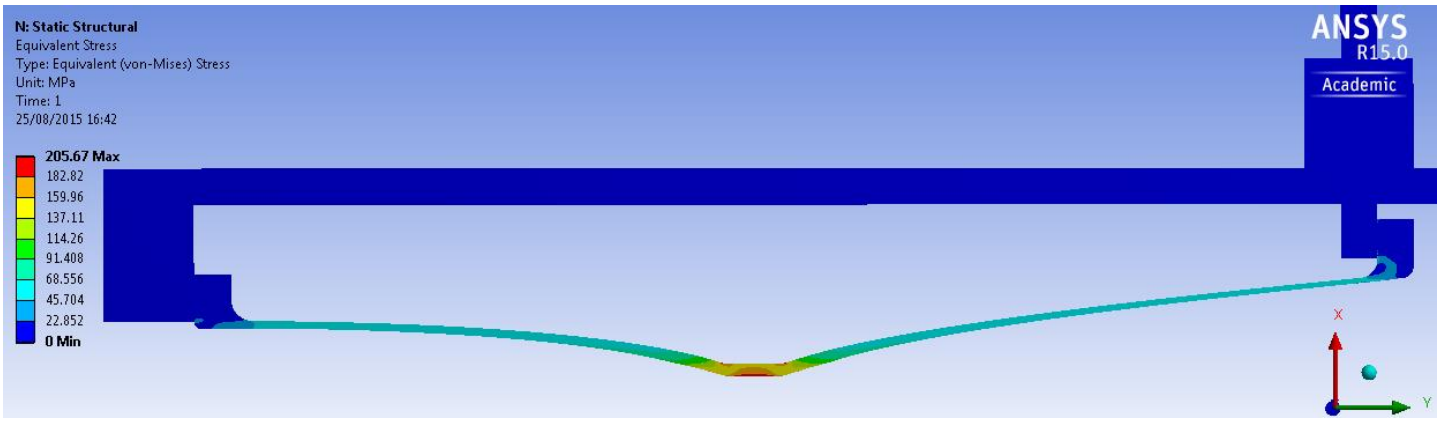

Figure 50 Von Mises equivalent stress distribution – Inner + outer conductor model

However, the dynamic behaviour of the horn is different, since in this case the contact between the inner and outer conductor leads to the attenuation (damping) of the oscillations. As an example, the following picture (Fig.51) shows how the axial displacement oscillations are almost completely damped after 250 ms:

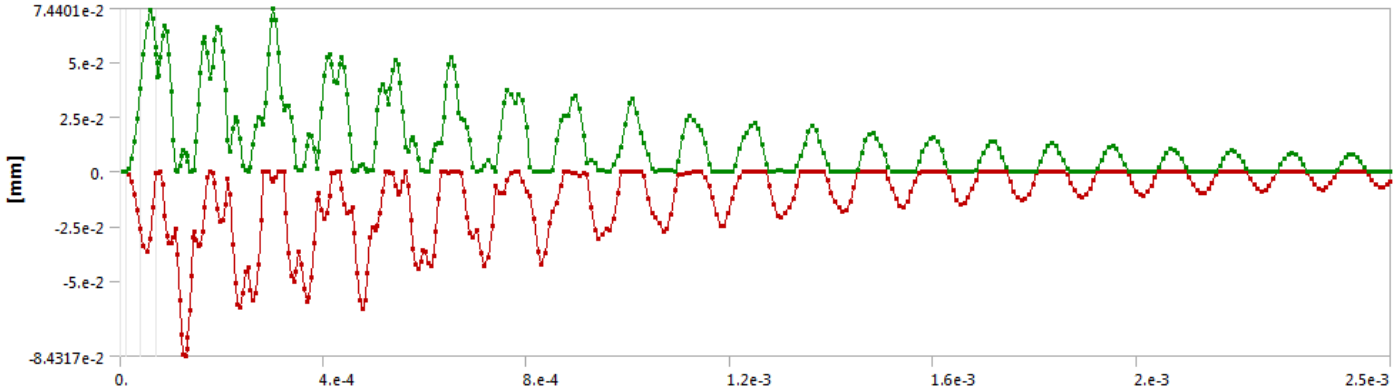

Figure 51 Axial displacement oscillations attenuation

7.4 Structural analysis conclusions

The results of the analysis carried out in this section are reassuring concerning the structural behaviour of the AD horn in the current operation. The range of displacements and stresses is within the acceptable limits of the material, and the buckling multiplicative factors are above the safety values. Furthermore, the lowest forced frequencies are way higher than the possible pulse frequencies, and it will be checked if they are also higher than the natural modes of the whole inner and outer conductor system.

It is important to consider that the temperature changes have not been taken into account in this analysis, the horn being loaded in this case only by electromagnetic body forces. The thermal stresses produced by the temperature increase in the horn would modify this results, and should be taken into consideration in the next studies. Moreover, the change of temperature modifies the structural behaviour of the horn, as the material properties change with the temperature. For that reason, a coupled analysis will be carried out in the future considering at the same time both thermal and structural loads.

However, the effects of the temperature gradient are weak compared to the ones of the electromagnetic pressure in the horn, therefore a relatively low variation towards higher compressive values is expected by including the thermal stresses in the horn.

8. Maxwell 3D®

In order to further cross-check the static properties of the horn, a different code has been used in order to analyse the effect of the magnetic forces on the horn structure. Maxwell 3D® is an Ansoft electromagnetic field simulation software, which is useful in our case for the calculation of the surface body forces and Joule heating generated by the electromagnetic field in the AD horn, while allowing an easy coupling with ANSYS® Workbench.

8.1 AD horn modelling in Maxwell 3D®

The inner conductor geometry is imported into Maxwell 3D®, where a magnetostatic analysis will be performed. A simulation region enclosing the geometry must be created, in order to specify a finite region where the FEM calculations are carried out. The current applied is the one corresponding to the maximum intensity (400 kA), and in this case it is not necessary to place a ground voltage, since a current excitation path will be specified instead (Fig.52).

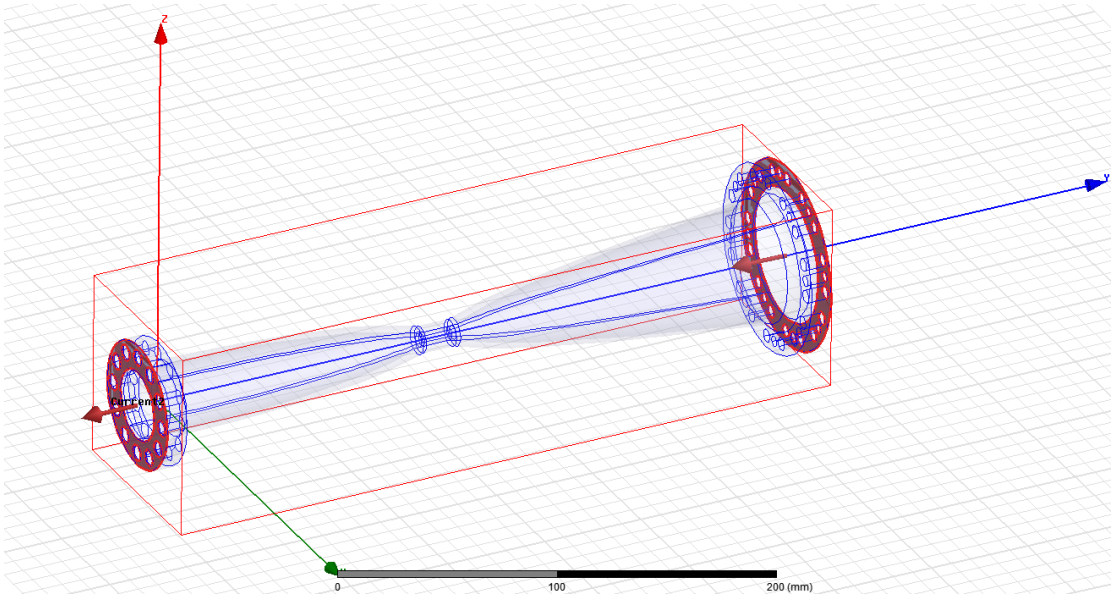

Figure 52 AD Horn geometry in Maxwell 3D®, simulation region and current path

The calculation of the electromagnetic body forces requires to define the Lorentz Force as a parameter of the simulation, and the 'Solution Setup' specifies the settings used for solving the simulation. Different meshing operations can be included for a more accurate solution, the meshing being less intuitive in Maxwell 3D® than in ANSYS® Workbench even if it is possible to obtain a quite refined mesh (Fig.53).

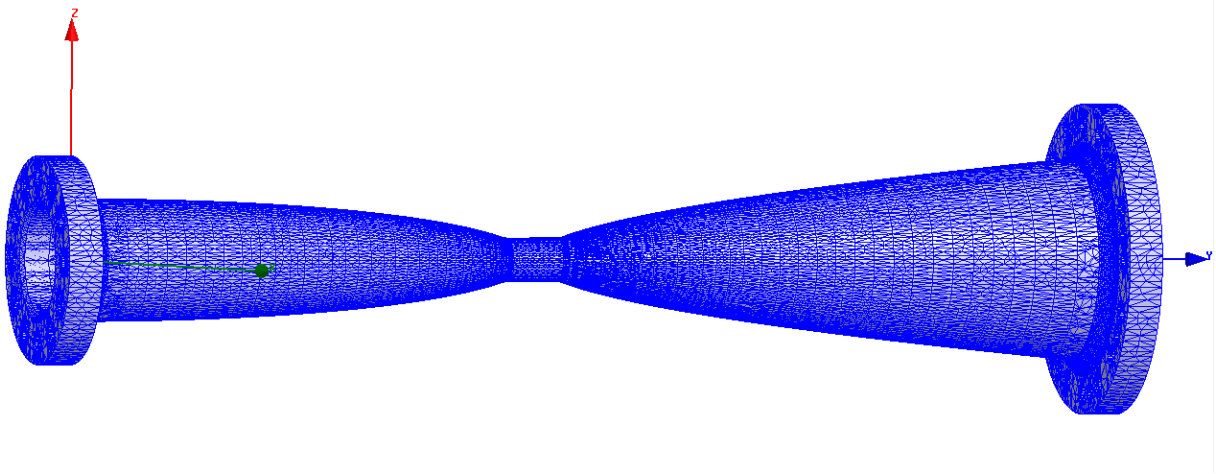

Figure 53 AD horn meshing in Maxwell 3D®

8.2 Electromagnetic body forces in Maxwell 3D®

As a result of the magnetostatic simulation we obtain the body forces distribution along the horn surface (Fig.54). This forces correspond to the pressure generated by the electromagnetic field, which was calculated previously by using formulas and the outer radius of the horn in function of each Y-coordinate. Obtaining the magnetic pressure along the horn with Maxwell 3D® is particularly interesting because the distribution is in this case continuous, instead of being applied to many different points as in the first analysis, where a tabular loading was used.

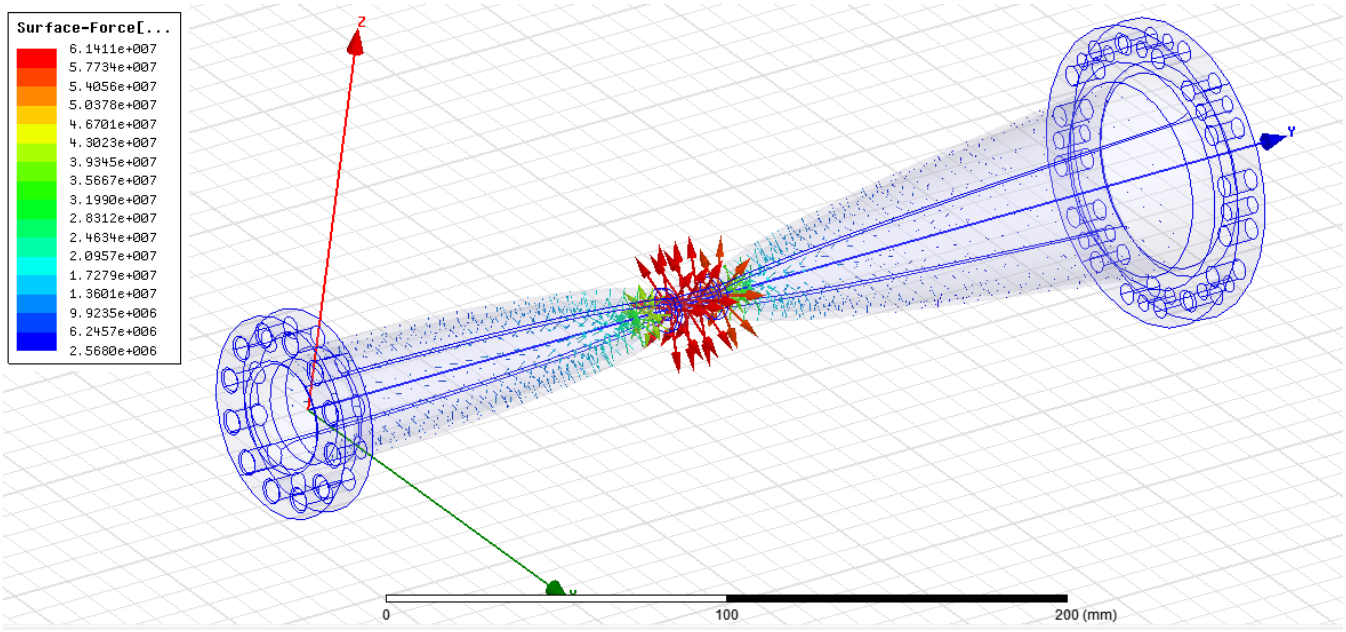

Figure 54 Maxwell® calculated electromagnetic surface forces in Pa

Moreover, the body pressure values correspond almost exactly to the calculated ones, since the maximum pressure applied is 61 MPa in the horn neck (2% difference with the calculated one) and the minimum pressure is 2.6 MPa in the wide end of the inner conductor (7% difference with the value obtained with the formulas). The electromagnetic force can be exported to a structural analysis in ANSYS® Workbench as 'Surface Body Pressure', the results being interpolated for the mesh created in Workbench; even if the meshes are different, the forces values are almost identical (Fig.55).

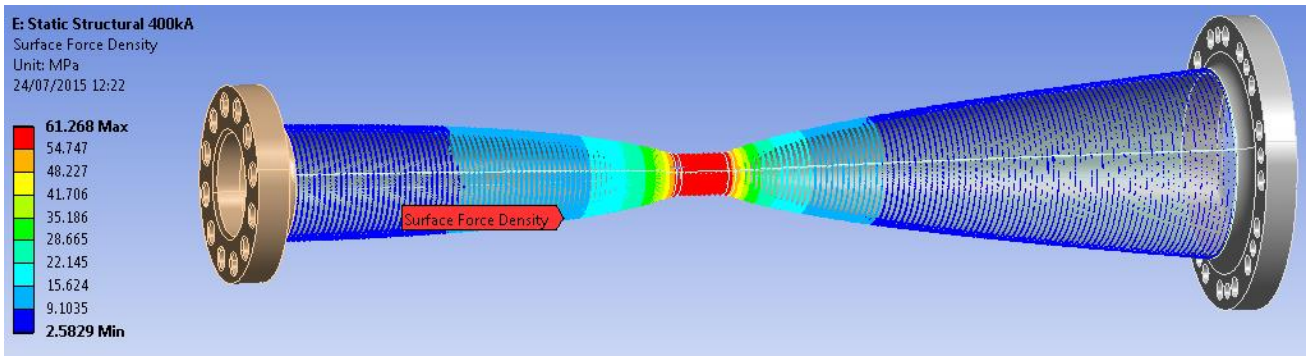

Figure 55 Surface body pressure imported in ANSYS® Structural from Maxwell 3D®

In this case, the whole horn model is used instead of the axisymmetric one, since the results have been obtained in the Maxwell three-dimensional version. Performing a static structural analysis with the imported pressure from Maxwell 3D® gives very similar results in terms of maximum stresses and displacements to the ones obtained with the tabular loading (maximum Von Mises equivalent stress: 205 MPa). However, since the meshes are substantially different in Maxwell 3D® and in Workbench, the stresses distribution is not so accurate in this case (Fig.56).

A transient dynamic analysis can also be carried out using the imported pressure from Maxwell 3D®, by applying the impulse of electromagnetic force as a triangular pulse lasting 60 µs. For that purpose, the procedure is identical to the previous one with Tabular Pressure, we will import the pressure distribution obtained in Maxwell with a ramped loading at 3 different time-steps, and by specifying different *Scale* values (0 or 1) the triangular pulse will be reproduced.

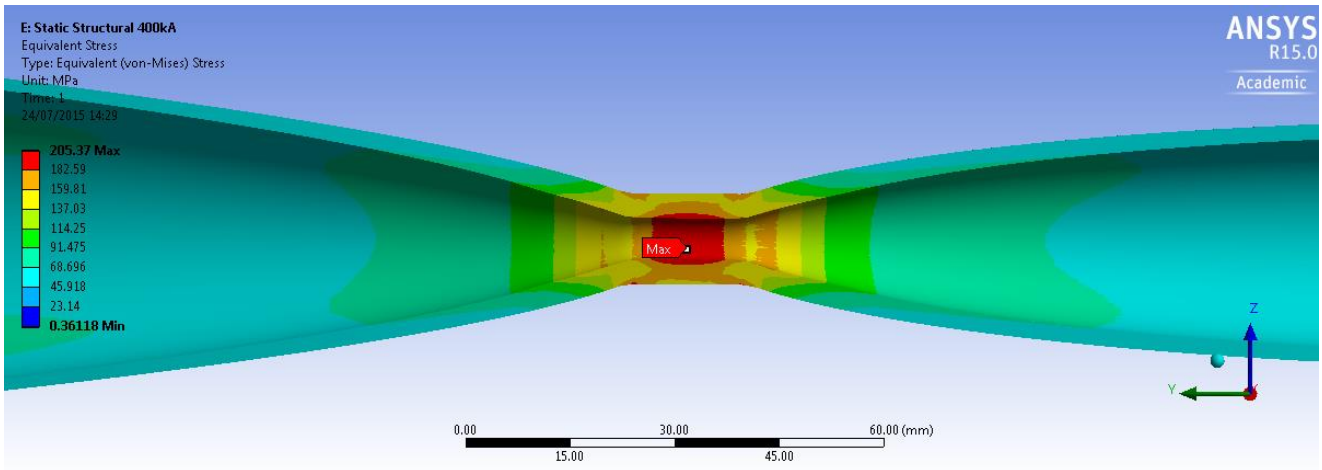

Figure 56 Von Mises equivalent stress distribution – Maxwell 3D® imported surface pressure

The results of stresses and displacements after the dynamic analysis are also very similar to the prior ones; as an example, the axial displacement values evolution and distribution along the horn and evolution displayed in the following picture is almost identical to the one obtained in the dynamic analysis of the previous section (Fig.57).

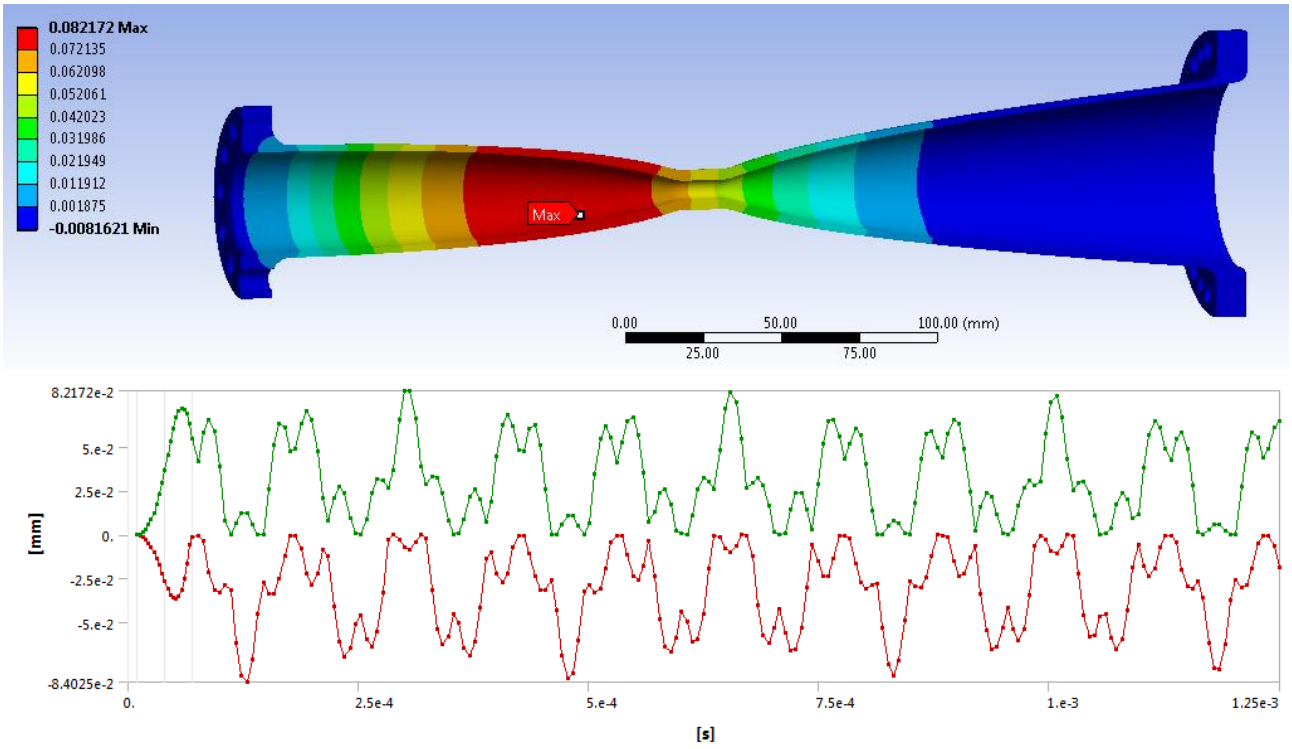

Figure 57 Axial displacement evolution and distribution along the AD horn in MPa
Transient dynamic analysis with imported Maxwell 3D® pressure loads

As a measure of the similarity in the results of the two approaches, the relative difference of the maximum values of axial displacement has been calculated for a few specific points. In table 5 are shown the relative differences between the maximum axial displacements reached for the Maxwell 3D® imported values and for the tabular loading performed in the axisymmetric model. The points considered belong to the outer surface of the inner conductor, and are identified in function of their Z coordinate, the origin being placed in the same location as in the horn drawings and 150 mm corresponding to the neck of the horn.

Table 5 – Maxwell 3D® imported pressure vs. tabular loading, maximum axial displacement comparison for few outer surface points

Z [mm]	Axial displacement [mm]		Relative difference (%)
	Tabular Pressure	Maxwell 3D®	
50	6.64E-02	6.36E-02	4.24
100	8.28E-02	8.15E-02	1.56
150	4.46E-02	4.58E-02	2.61
200	7.03E-02	7.05E-02	0.31
250	5.84E-02	5.97E-02	2.22

8.3 Thermal results in Maxwell 3D®

The Joule heating values in the inner conductor are given as 'Ohmic Losses', an outcome of the magnetostatic analysis in Maxwell. The values obtained and the distribution of the Joule heating are very similar to the ones obtained with ANSYS® Electric (Fig.58).

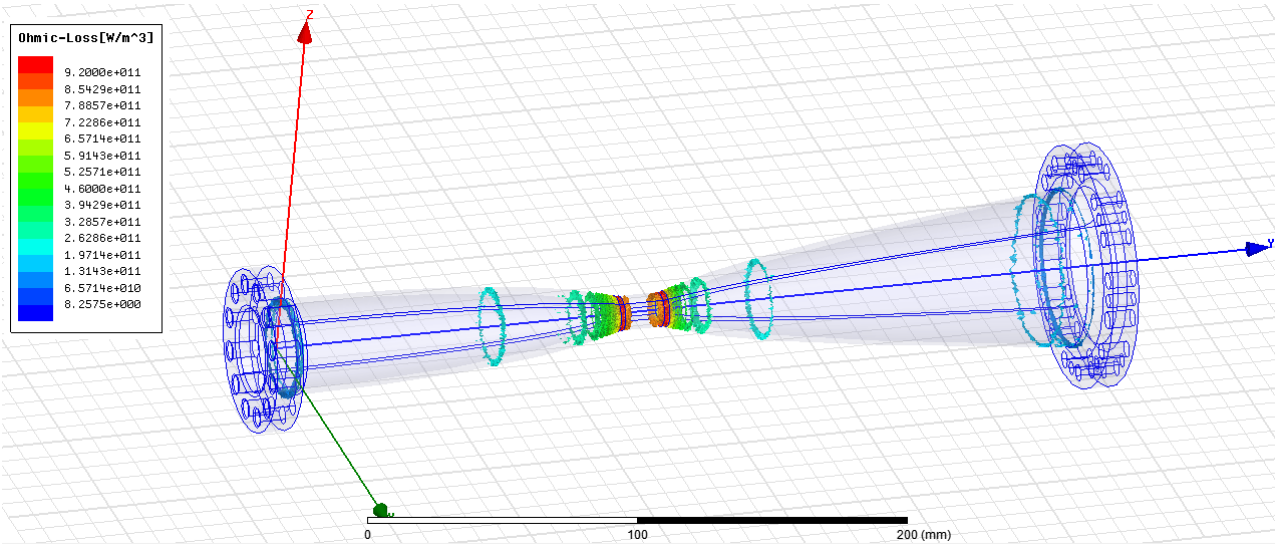

Figure 58 Ohmic losses (Joule heating) in the AD horn under maximum intensity current

The total heat generated by the current pulse at maximum intensity can be calculated through the *Field Calculator* feature, by integrating the Ohmic Losses over the volume of the horn. The resulting total heat generated is 13.7 MW, which is of the same order as the ones calculated in the previous sections.

This results can be then coupled with a transient thermal analysis, where they are imported as *Internal Heat Generation.* The accuracy of the interpolated values imported from Maxwell 3D® is given by the Scaling Factor specified in the *Transfer Summary*, which shows a quite high precision in the mapping from one mesh to the other (capture shown in Figure 60). However, the thermal coupling will only take into account the maximum intensity (the one specified in Maxwell), and not the complete pulse shape as considered in the electric analysis in Workbench.

Exporting Volume Loss Density With Scaling...

Object	Total Loss	Scaling Factor
horn	1.37391E+007W	0.998529

Figure 60 Imported load transfer summary for the thermal coupling from Maxwell 3D®

8.4 Conclusions on the use of Maxwell 3D®

Concerning the structural results, Maxwell 3D® allows to obtain a continuous pressure distribution, which is a more accurate approach than the pressure calculation with formulas. On the other hand, this accuracy is worsened by the coupling with different meshes, and for that reason this software will be mainly used to verify the pressure values analytically calculated through the formulas.

As for the thermal results, the procedure is much simpler in terms of meshing and current pulse reproduction with ANSYS® Electric than with Maxwell 3D®, thus the software will be used for crosschecking the Joule heating distribution and the total heat generation in the AD Horn.

9 General conclusions and next steps

This note describes the current understanding via simulations of the AD horn thermomechanical and electro dynamic behaviour. From the thermal studies carried out it is possible to conclude that in this preliminary simulations the temperatures reached in the AD horn during operation are acceptable in the present case, but could be problematic in the future, especially with the increase of the pulse repetition rate. The structural analysis performed have shown that the AD horn response under the electromagnetic pressure generated is within the safe limits of the material in terms of maximum static and dynamic stresses, buckling, and modal frequencies.

Additional studies will be performed in order to clarify the open points left open in this study. As a first step, the whole model of the AD horn system will be used, including the inner conductor, the outer supports and the strip-line. With this model we will be able to simulate the thermal behaviour of the magnetic horn and the surrounding parts. The beam energy deposition in the outer conductor can also be considered in the next simulations for a more accurate approach.

In the whole model the heat conduction through all the external parts will be taken into account. The thermal conductance must be evaluated though, since considering a perfect conduction between the inner and outer conductor as done in the present study is a very optimistic approach.

Furthermore, the convection values considered in the current analysis are definitely too conservative, therefore the heat convection coefficient will be calculated in the future through detailed CFD calculations, by simulating the complete air cooling system of the horn.

Finally, many properties of the horn material change with the temperature variation, then the system requires of a coupled analysis taking into account at the same time the electrical, structural and thermal properties of the material. We need to perform a coupled Electric-Thermal-Structural analysis in order to take all the property variations into consideration and obtain more precise results.

The AD horn test bench that will be carried out in the future will allow to validate many results of these simulations, since the temperatures and the stresses reached in the device will be measured during a long operation period, under high repetition rates of the current pulse (although the effects of the beam energy deposition will not be considered in the test bench).

Acknowledgements

We are very grateful to EN/MME for supporting this work, especially to B. Riffaud and M. Garlasche for their collaboration.

References

[1] D. Boimond, M. Frauchiger, T. Kurtyka, M. Lubrano di Scampamonte, R. Maccaferri, S. Maury, L. Nikitina, J.-C. Schnuriger, *Consolidation of the 400kA magnetic horn for AAC antiproton production*, s.l.: CERN/PS 94-02 (AR), 06.05.1994

[2] M.Calviani, *400 kA magnetic horn inner conductor drawings*, [online] 16.01.2012 https://edms.cern.ch/document/1180248/1

[3] S. Sgobba, private communication

[4] M. Calviani, *Impact of future AD beam parameters for target area*, Presentation at 147th IEFC Committee meeting, 28.08.2015 https://indico.cern.ch/event/439999/contributions/1142827/1637564/mc__impact_AD-target_beam_parameters__August2015_v3.pptx

[5] MPDB v.7.71, JAHM Software Inc., 2014; software available at http://www.jahm.com

[6] T.T. Böhlen, F. Cerutti, M.P.W. Chin, A. Fassò, A. Ferrari, P.G. Ortega, A. Mairani, P.R. Sala, G. Smirnov and V. Vlachoudis, *The FLUKA Code: Developments and Challenges for High Energy and Medical Application*, Nuclear Data Sheets 120, 211-214 (2014)

[7] A. Ferrari, P.R. Sala, A. Fassò, and J. Ranft, *FLUKA: a multi-particle transport code*, CERN-2005-10 (2005), INFN/TC_05/11, SLAC-R-773

[8] B. Riffaud, private communication

I. Annex A: ANSYS Parametric Design Language (APDL) Coding

1) Calculation of the total heat generated by the current pulse

```
SET,,,,,6.71e-005                          !! Set time of current peak

*DIM,hgenerat,ARRAY,nelem                  !! Create tables for heat
*DIM,volume,ARRAY,nelem                    !! generation, volume and
*DIM,totheat,ARRAY,nelem                   !! total heat in W

*DO,i,1,nelem                              !! Get these values from each
      *GET,hgenerat(i),ELEM,i,JHEAT,,      !! element and store them in
      *GET,volume(i),ELEM,i,VOLU,,         !! the created tables

      totheat(i)=hgenerat(i)*volume(i)     !! Multiply to obtain total heat
*ENDDO

*CFOPEN,D:\Convection\Jheat,txt            !! Write the values in a txt file
*VWRITE,hgenerat(1,1,1),volume(1,1,1),totheat(1,1,1)
(g16.8,g16.8,g16.8)
```

2) Application of two heat generations: Joule heating and beam energy deposition

In order to perform a transient thermal analysis considering the thermal effects of both the current pulse and the beam interaction with the horn, it is necessary to use APDL commands which allow to include two heat generation distributions at the same time.

Firstly, the Joule heating generated by the current pulse is saved into tables, one table for each time-step, each table containing the Joule heating values for each element. In order to have an accurate shape for the Joule heating evolution, the time-steps are divided in four parts, and defined in the pre-processor with help of the following commands:

```
*DO,TIME1,0,16,1          !!First Part
      TIME,5E-5+TIME1*0.1e-5
      SOLVE
*ENDDO
*DO,TIME2,0,1,1           !!Second Part
      TIME,6.66E-5+TIME2*0.05e-5
      SOLVE
*ENDDO
*DO,TIME3,0,12,1          !!Third Part
      TIME,6.8E-5+TIME3*0.1e-5
      SOLVE
*ENDDO
*DO,TIME4,0,11,1          !!Fourth Part
      TIME,8.5E-5+TIME4*1e-5
      SOLVE
*ENDDO
TIME,2e-4                 !!Last step
```

We can notice that the second part, corresponding to the current peak, lasts 500 ns (from 66.6 µs to 67.1 µs), as the beam energy deposition values will be added to the Joule heating values stored in those time-steps (Fig.A1).

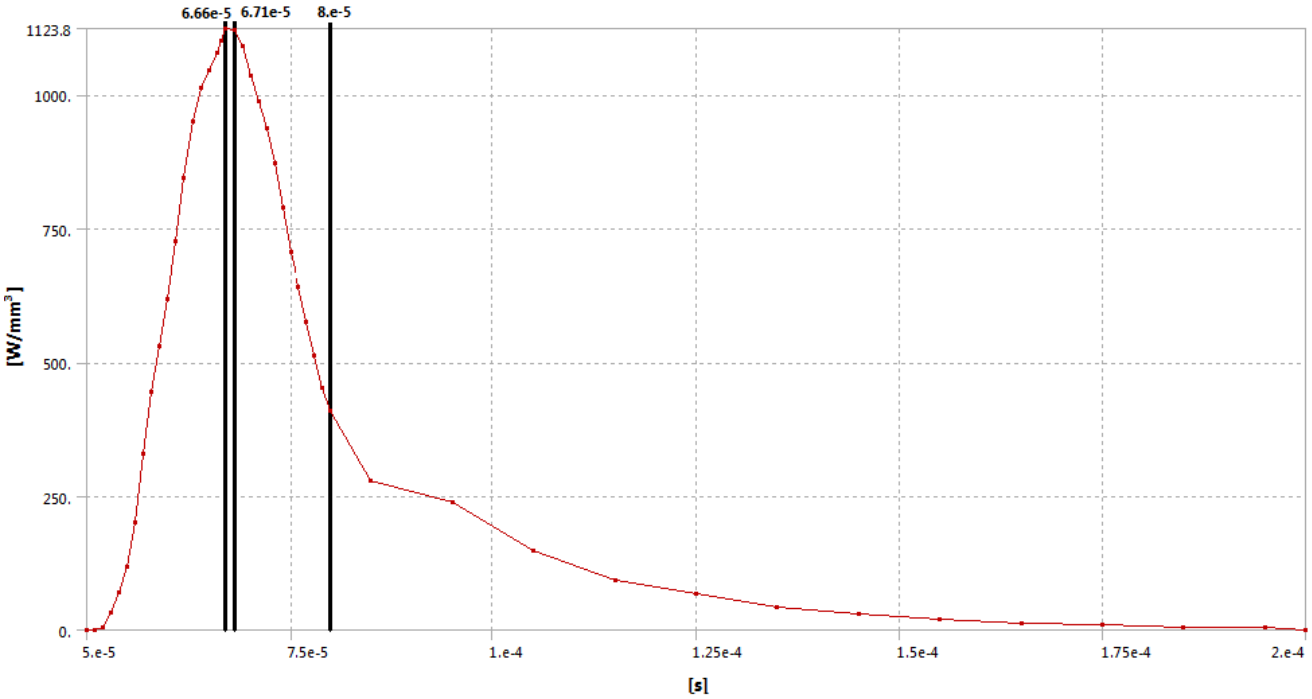

Figure A1 Time-steps defined in the preprocessor

In the post-processor, the Joule heating for each element is saved into tables, one table per time-step:

```
/post1
ESEL,all
*GET,nelem,ELEM,0,count              !! Get the number of elements
Loadstep=1e-6                        !! Define the desired time-step
*DO,t,0,16,1                         !! First Part
    SET,,,,,5e-5+t*Loadstep          !! Set the time-step considered
    *DIM,hgeneration,ARRAY,nelem     !! Create a table named hgeneration
    *DO,i,1,nelem
       *GET,hgeneration(i),elem,i,JHEAT,, !!Store the Joule Heat values
    *ENDDO
    *CFOPEN,D:\hgenA%t%,txt          !! Open txt file named hgenA1, hgenA2…
    *VWRITE,hgeneration(1,1,1)       !! Write the data into the .txt file
      (g16.8)
*ENDDO
```

The set of tables corresponding to the first part will be named *hgenA0*, *hgenA1*…and we proceed the same way for the second part defining the tables as *hgenB0* and *hgenB1*, for the third part *hgenC0*, *hgenC1*… and for the fourth part *hgenD0*, *hgenD1*…

The next step is obtaining the values of the beam heat generation for each element into a table to be able to sum them with the tables obtained for the Joule heating. For that purpose, we run a thermal analysis importing the energy deposition from FLUKA and applying in the post-processor a similar APDL code:

```
*GET,nelem,ELEM,0,count
*DIM,hgenerat,ARRAY,nelem
*DO,i,1,nelem
      *GET,hgenerat(i),ELEM,i,HGEN,,       !! Save the heat generation
*ENDDO                                     !! values for each element
*CFOPEN,D:\ENERGYDEP,txt                   !! into a ENERGYDEP.txt file
*VWRITE,hgenerat(1,1,1)
  (g16.8)
```

At this point, the heat generation values are re-applied to all the elements and the transient thermal analysis is performed. It is necessary to sum up the beam-induced heat generation table to the two Joule heating tables corresponding to the current peak (*hgenB0* and *hgenB1*), while for the first, third and fourth part we only need to apply the Joule heating values stored in the tables *hgenA*, *hgenC* and *hgenD*. The next code extract shows the commands used for the first and second part, the procedure for the third and fourth part being the same as for the first one.

```
*DO,t,0,16,4
      *DIM,HG%t%,ARRAY,nelem            !!Read the first set of tables hgenA
      *VREAD,HG%t%(1),D:\hgenA%t%,TXT   !!Save the data in tables HG1, HG2,…
       (G16.8)
      TIME,5E-5+t*0.1E-5                !!Specify the time-steps
      ESEL,all
      *DO,i,1,nelem
            ESEL,s,ELEM,,i
            BFE,all,HGEN,,HG%t%(i)      !!Apply the stored Joule Heat
            ALLSEL
      *ENDDO
      KBC,0                             !!Apply the loads as ramped
      SOLVE
*ENDDO

*DIM,ENERGY,ARRAY,nelem                       !! Read the table containing
*VREAD,ENERGY(1),D:\ENERGYDEP,txt             !! the energy deposition
(g16.8)
*DO,t,0,1,1
      *DIM,HG%t%,ARRAY,nelem                  !! Second set of tables with
      *VREAD,HG%t%(1),D:\hgenB%t%,txt         !! Joule Heat values (hgenB)
      (g16.8)
      *DIM,HGtotal%t%,ARRAY,nelem
      *DO,j,1,nelem                           !! Create a table with the
            HGtotal%t%(j)=ENERGY(j)+HG%t%(j)  !! Total Energy Deposition
      *ENDDO
      TIME,6.66e-5+t*0.05e-5                  !! Specify time-steps
      ESEL,all
      *DO,i,1,nelem
            ESEL,s,ELEM,,i
            BFE,all,HGEN,,HGtotal%t%(i)       !! Apply the total energy
            ALLSEL
      *ENDDO
      KBC,0
      SOLVE
*ENDDO
```

3) Application of the thermal loads for a steady-state thermal analysis

This example shows how the Joule heating and beam energy deposition are applied for a steady-state analysis considering the "accumulation mode" beam parameters [4]:

```
esel,all
*get,nelem,elem,0,count              !! Get the number of elements

*DIM,ENERGY,array,nelem              !! Insert in ENERGY the data of the
*VREAD,ENERGY(1),D:\ENERGYDEP,txt    !! energy deposition for each element
 (g16.8)
*DIM,HG,array,nelem            !! Insert in the table HG the maximum Joule
*VREAD,HG(1),D:\hgenB1,txt     !! heat data for each element (which is
 (g16.8)                       !! stored in hgenB1)
Npulses=5                      !! Accumulation mode considered (5 pulses,
cycletime=148                  !! one each 15.6 seconds, and 70s cooling)

*DIM,HGtotal,array,nelem       !! Table storing the total energies
*do,j,1,nelem
      HGtotal(j)=((ENERGY(j)*500e-9)+(HG(j)*20e-6))*Npulses/cycletime
*enddo
esel,all
*do,i,1,nelem
      esel,s,elem,,i
      bfe,all,hgen,,HGtotal(i)       !! Apply the energy to all elements
      allsel
*enddo
```

II. Annex B: Inner conductor Metrology Review

Metrology tests carried out in the existing inner conductor have shown that the horn shape is slightly different from the plans of the latest design. By reconstructing the shape of the inner conductor, we want to study if the variation is due to the fact that the analysed horn corresponds to another existing drawing or simply that the tolerances were not respected correctly.

Comparing the different drawings of the horn [2], the external shape is almost identical in all of them. The main difference is the radius in the middle part which is 6 mm or 7 mm in the old drawings, and 6.5 mm in the new design. As an example, in the following figure we can see a comparison of the external shape of two old drawings (*PS-C-6517-60* and *PS-C-6601-60*) and the latest design (*PS-C-6600-60*) (Fig.B1).

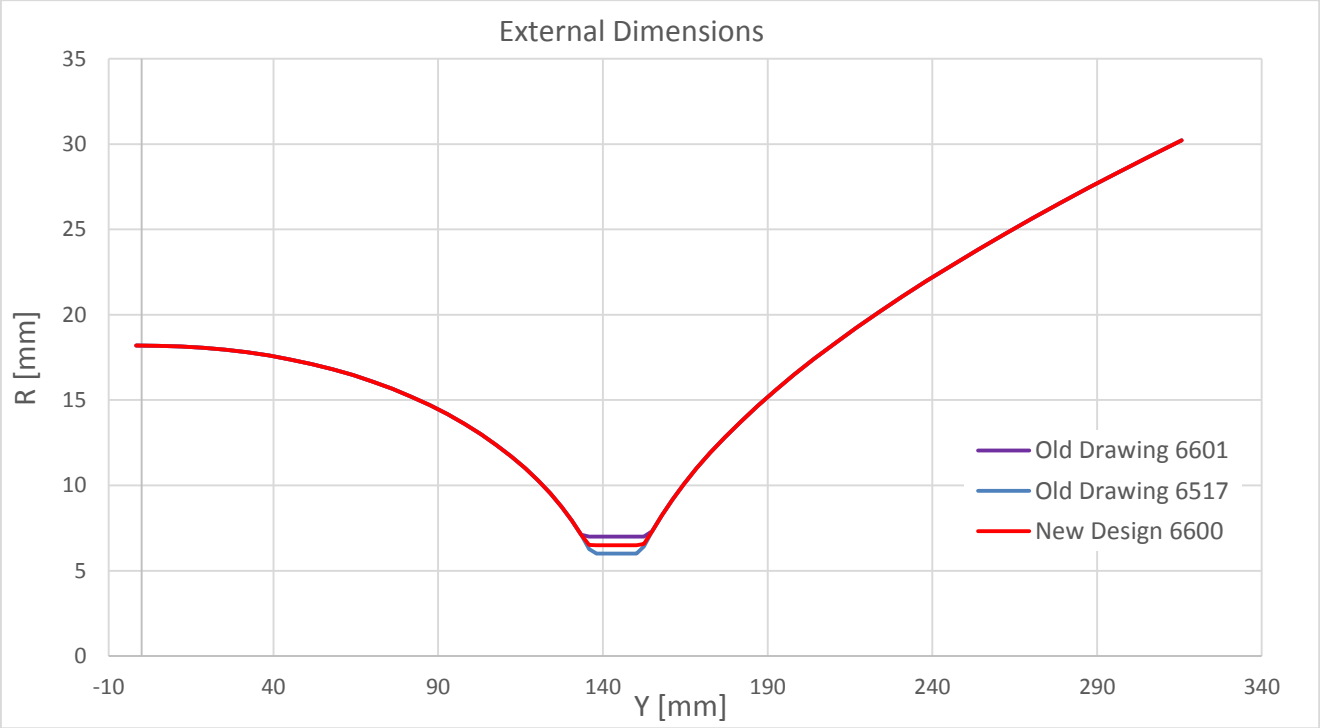

Figure B1 External shape of the inner conductor according to different drawings

According to the metrology results the external radius in the middle part is 6.5±0.02 mm, so the measured horn corresponds most probably to the new design.

The internal shape of the measured horn can be compared to the drawings too, by interpolating the measurements with the dimensions given in the drawings. The error percentage between the measures and the different radius specified in the drawings is calculated as:

$$\frac{R_{metro} - R_{drawing}}{R_{metro}}$$

As can be seen in the picture below, where the internal dimensions of different drawings of the inner conductor are compared, the lowest error in the internal shape corresponds to the latest design (Fig.B2).

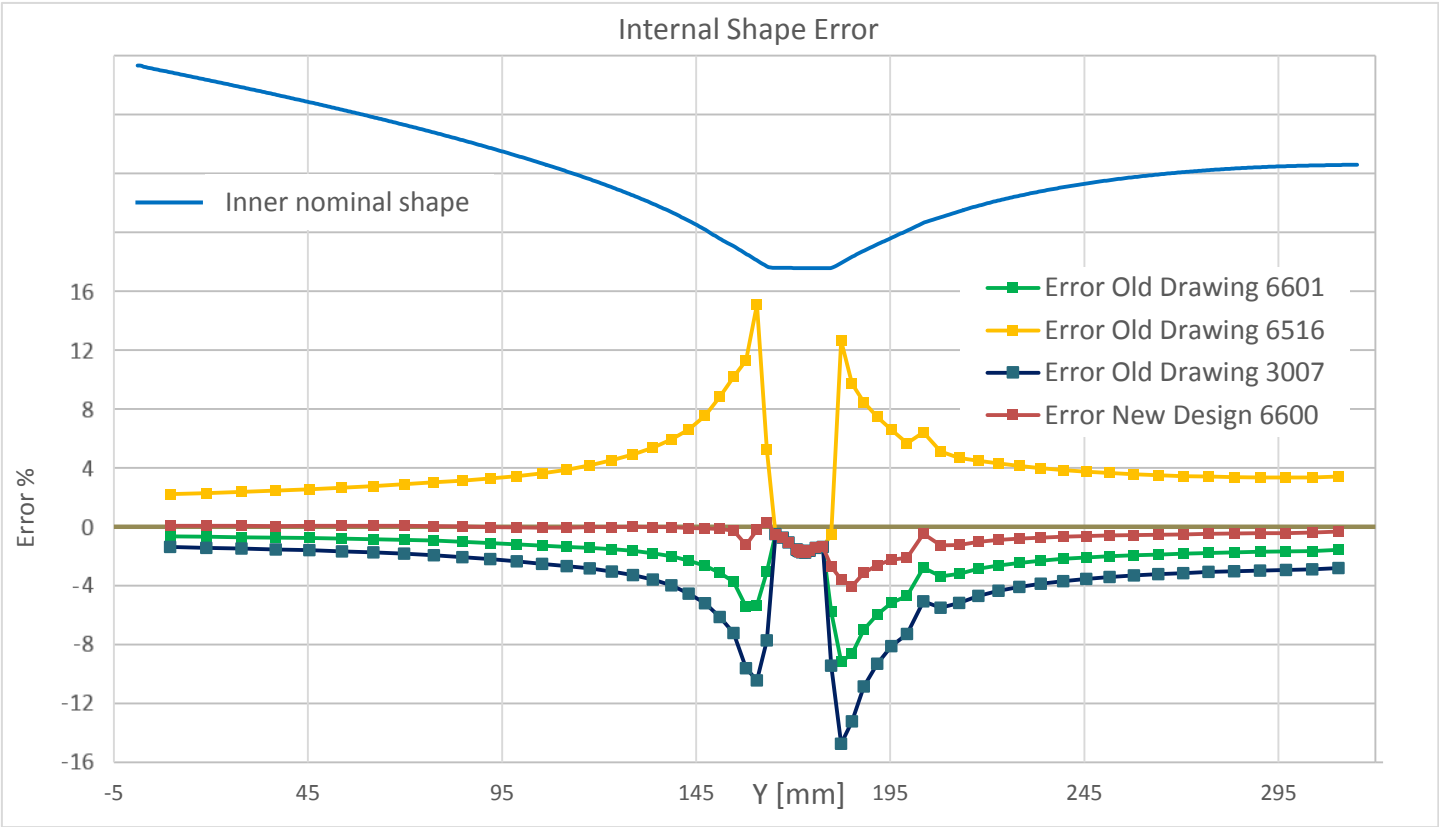

Figure B2 Comparison of the internal shape error for different horn drawings

Thus, we can conclude that the measured horn corresponds to the latest design *PS-C-6600-60-2C*, with a variation up to 4% in the internal part and 2% in the external one (Fig.B3), the variation is due to the fact that the tolerances were not correctly respected.

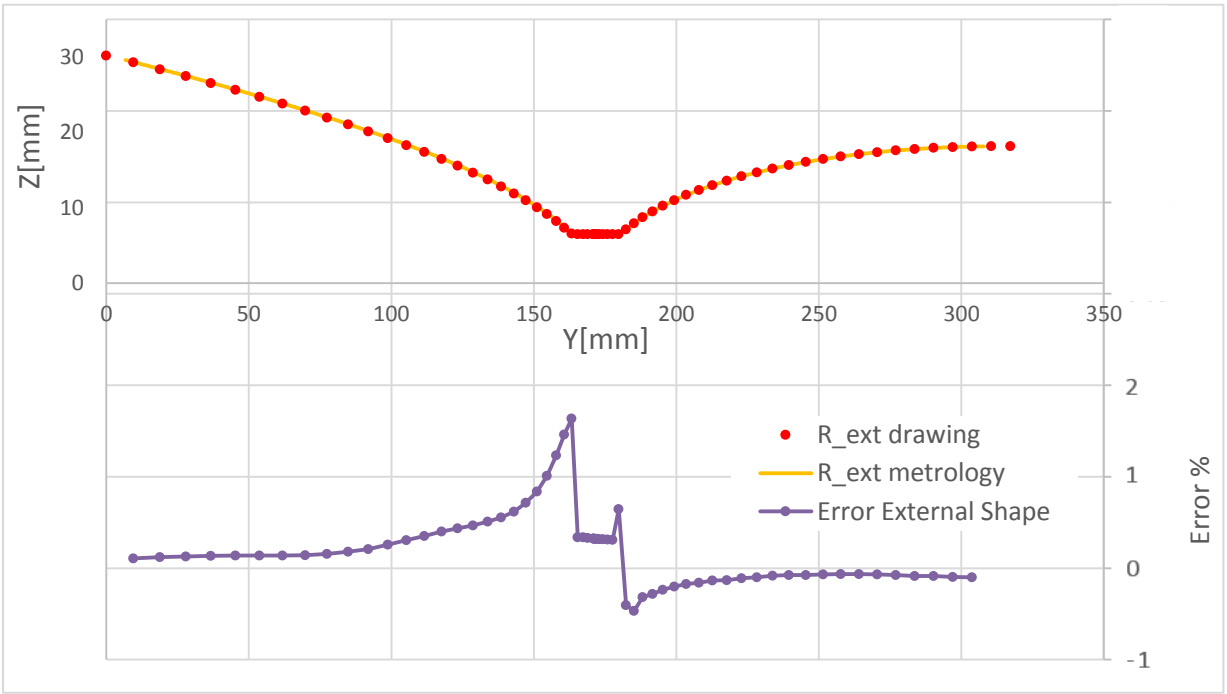

Figure B3 External radius error between metrology results and horn drawing dimensions
Maximum error = 2%